Spin Coherence Excitation in Pr^{3+}:Y_2SiO_5

Master's Thesis
by
Fredrik Vestin

Lund Reports on Atomic Physics, LRAP-297
Lund, February 2003

Abstract

This master's thesis investigates the ground state hyperfine levels coherence time in Pr^{3+}:Y_2SiO_5. This property is important for the future development of quantum computers based on this or similar crystals. A suitable method to measure the coherence time at liquid helium temperature for two hyperfine levels in the $^4H_3$ level of Pr^{3+} was developed and the coherence time has also been determined approximately to 540 μs.

Examensarbetet undersöker koherenstiden för två hyperfin nivåer i grundtillståndet för Pr^{3+}:Y_2SiO_5. Detta är en egenskap som är viktig för en framtida kvantdator baserad på denna eller liknande kristaller. En metod att mäta koherenstiden vid flytande helium temperatur för två av hyperfinnivåerna i grundtillståndet för Pr^{3+} har utvecklats och koherenstiden har med denna metod mätts upp till 540 μs.

Contents

Chapter 1

Introduction

As classical computers are reaching their limit of performance, quantum computers are merely taking form. The difference between classical and quantum computers is due to the superposition. I find the idea of superpositions quite bothersome sometimes. There are many consequences just because a quantum systems can be in a superposition, like the fact that doing a measurement would collapse a superposition. What happens when you collapse something? When does the superposition really collapse? Does the superposition ever collapse? Imagine that you are going to do a measurement on a quantum state that is supposed to be in a superposition of quantum states Φ_1 and Φ_2. Measuring Φ_1 does in this case mean that you get '1' blinking on your screen and measuring Φ_2 gives you '0'. All is fine and you measure one of those numbers and collapse this quantum state. That is one way of looking at the problem. An other way, which I think is very disturbing, is to say that by doing the measurement you yourself become a superposition of having measured a '1' or a '0'. Since it is no fun walking around being a superposition you tell your colleagues that you measured either a '1' or a '0'. So now they also become part of the same universe as you, assuming that the other you of the superposition tell that you measured the opposite. Assuming that this happen all the time, without us even having to do measurements, we would then end up with infinitely many realities or universes.

One interpretation of this is that we must be living in an infinite parallel universe. Or is there something fundamental about quantum physics that we do not yet know? Maybe it does not work, as we would expect it to if there are too many particles involved. When, if ever, does the physics of quantum mechanics start to go bad? That is one question that I would like to get the answer on. The best candidate to answer this question could be a quantum computer, since it is inherently a quantum system. After waving his hand for several lectures and doing all sort of math magic your quantum mechanics teacher comes up with a wave function that describes a hydrogen atom. All good, it describes the atom precisely and experiments have proved quantum mechanics to be the right model to use. But that is about the limit when you want to describe a quantum state exactly using equations only. When you start doing more com-

plicated calculations involving more particles than two, you have to start using perturbation methods and assume things. The perturbation you used and the things that you assumed then limit the result of a calculation. The life of atoms are once again hazy and hard to understand completely, but usually quite easy to predict. As in other many-body systems you have to do simulations. A task that becomes impossible if you make a simulation of a quantum system on a normal computer. A large scale quantum computer might on the other hand be able to stand up against this challenge, not today but possibly in the future.

This thesis is organised in the following way. In chapter two I explain the underlying physics for many of the concepts I use later in the report. It is not necessary to read chapter two carefully for someone that rather just accept the phenomena that are explained using the Bloch vector formalism. Chapter three describes an experimental method that is commonly used within this field, namely photon echoes. I advise you to understand the photon echo process, otherwise you will have a hard time when you read about my experiments. Chapter three also explains the phenomena that introduce decoherence in a rare-earth doped crystal. Chapter four is a general overview of quantum computers and should be understood by most people without any former knowledge in this area. Chapter five explains the rare-earth-doped crystal quantum computing scheme in more detail. It also explains the properties of the crystal I have been working with. Chapter six is a summary of the equipment I have used and how I have used it. Chapter seven, eight and nine explain the different experiments that I have tried. Chapter nine is the most important, since it describes the experiments that gave me the results. But doing the experiment have been a continuous process and one experiment has lead to the other. The report has been written during the last six months and can be seen as chronicle of my work. And what I (you) did not understand in one experiment might be explained in the next, but it is likely that it will not be explained at all. The focus, throughout the experiments, has been on finding a technique for measuring the coherence time for the hyperfine levels in the groundstate. I have tried to avoid sidepaths as much as possible and the bad experiments have been trashed without fully knowing the mechanisms that made them not work. This might sound like I have been working with blinds all the time, but I have been quite sceptical about my experiments at time and I have had to design new experiments, since I have come up with alternative explanations for my data.

Fredrik Vestin

Chapter 2

Quantum Physics

2.1 History

Until the end of the nineteenth century, classical physics appeared to explain all physical phenomena. Particles obeyed Newton's laws of motion and Maxwell's equations of electromagnetism. In 1905 A. Einstein introduced his theory of special relativity for particles that move at velocities near the speed of light. A few famous experiments made scientist of the early 1900s to begin to question classical physics. These were the discovery of the photoelectric effect, the Compton effect, black-body radiation and the Stern-Gerlach experiment among others. The concept of quantisation and wave-particle duality was born. One equation, a wave function and a few postulates were identified and said to be able to completely describe the state of a physical system. The quantum mechanical description is basically a mathematical way of describing nature and is merely a guess based on intuition and experience. Even if more than a century has gone, it has not been proved wrong yet.

2.2 Quantum representation using density matrices

A quantum system is described by its wave function, usually denoted Ψ and it contains all information about the system. There is a linear and Hermitian operator $\hat{A}$ associated with every dynamical physical observable variable $\langle A \rangle$. The only result of a precise measurement of the dynamical variable is one of the eigenvalues a_n of the Hermitian operator $\hat{A}$ operating on Ψ as

$$\langle A \rangle = \int \Psi^* \hat{A} \Psi d^3r \tag{2.1}$$

Dirac formulated a concise and convenient formalism for making quantum mechanical calculations. The wave function comes in two flavours the *bras* and

the *kets*. They contain identical information and are adjoint vectors in the Hilbert-space that those vectors span. The *ket* is written $|\Psi>$ and the *bra* is written $<\Psi|$. The wave function can contain information that has no classical counterpart. It can be in a superposition of states and have a probability amplitudes c_n that are complex numbers that gives a phase between the states. A superposition of states can thus be written:

$$|\psi> \quad = \quad \sum_n c_n|\phi_n> \tag{2.2}$$

with

$$\sum_n |c_n|^2 \quad = \quad 1, \tag{2.3}$$

where $|c_n|^2$ is the probability of observing the system in state ϕ_n. When you have determined the state of the quantum system it looses its property of superposition and collapses to only one state. Further measurements will only yield ϕ_n with probability $|c_n|^2 = 1$. The time and spatial evolution of the quantum system is described by the time-dependent Schrödinger equation

$$i\hbar\frac{\partial}{\partial t}|\Psi(t)>= \hat{H}|\Psi(t)> \tag{2.4}$$

where H is the Hamiltonian, or total energy operator of the system. The wave function can be expanded in its spatial and time dependent parts as

$$\Psi(\vec{r},t) = \sum c_n(t)u_n(\vec{r}), \tag{2.5}$$

Where $c_n(t)$ is the temporal evolution of the state and $u_n(\vec{r})$ the Hamiltonian basis wave functions. The Hamiltonian basis wave functions are assumed to be orthonormal so that they obey the relation

$$\int u_m^*(\vec{r})u_n(\vec{r})d^3r) = \delta_{mn} \tag{2.6}$$

where δ_{mn} is the *Kronecker delta*. Inserting (2.5) into the Schrödinger equation (2.4) we obtain

$$i\hbar\sum_n \frac{\partial c_n(t)}{\partial t}u_n(\vec{r}) = \sum_n c_n(t)\hat{H}u_n(\vec{r}) \tag{2.7}$$

Multiplying both sides with u_m^* and integrating over all space now yields

$$i\hbar\frac{\partial c_n(t)}{\partial t} = \sum_n c_n(t)H_{mn} \tag{2.8}$$

where

$$H_{mn} = \int u_m^*(\vec{r})\hat{H}u_n(\vec{r})d^3r) \tag{2.9}$$

This equation is equivalent to the Schrödinger equation (2.4) but is only written in terms of the probability amplitude $c_n(t)$ of the orthonormal eigenfunctions n for the state. Omitting the spatial part, the quantum state can now be expressed as

$$|\Psi>= \begin{bmatrix} c_0(t) \\ c_1(t) \\ \vdots \\ c_{n-1}(t) \end{bmatrix} \tag{2.10}$$

The expectation value of an operator A is hence in terms of $c_n(t)$

$$\langle A\rangle = \int \Psi^* \hat{A}\Psi d^3r = <\Psi\,|\hat{A}|\Psi> = <\sum_n c_n(t)\,|\hat{A}|\sum_m c_m(t)> = \sum_{nm} c_n^* c_m A_{nm} \tag{2.11}$$

With regard to this equation we introduce the *density matrix*

$$\rho_{nm} = c_n^*(t)c_m(t) = |\Psi><\Psi\,| \tag{2.12}$$

Or usually it is expressed as an ensemble average as

$$\rho_{nm} = \overline{c_n^*(t)c_m(t)} = |\Psi><\Psi\,| \tag{2.13}$$

The physical interpretation of $\hat{\rho}$ is that the diagonal elements (ρ_{nn}) of the matrix give the probability that the system is in an energy eigenstate n. The off diagonal part ($\rho_{mn}, m \neq n$) gives the coherence between levels n and m. The expectation value in terms of ρ_{nm} is now written

$$\langle \bar{A}\rangle = \sum_{nm} \rho_{nm}A_{mn} = \sum_n (\sum_m \rho_{nm}A_{mn}) = \sum_n (\hat{\rho}\hat{A})_{nn} = tr(\hat{\rho}\hat{A}) \tag{2.14}$$

The time evolution of the density matrix (2.12) is given by

$$\frac{d\rho_{nm}}{dt} = c_n^*\frac{dc_m}{dt} + c_m\frac{dc_n^*}{dt} \tag{2.15}$$

Using the result from (2.9) we can write the time evolution as

$$\begin{aligned} \frac{d\rho_{nm}}{dt} = \frac{-ic_n^*}{\hbar}\sum_k c_k H_{mk} + \frac{ic_m}{\hbar}\sum_k c_n H_{kn} = \\ \frac{i}{\hbar}\sum_k (\rho_{km}H_{mk} - H_{kn}\rho_{nk}) = \frac{i}{\hbar}\left[\hat{\rho},\hat{H}\right]_{nm} \end{aligned} \tag{2.16}$$

This is the *Liouville equation.* It only describes how the density matrix evolves in time as the result of interactions that are included in the Hamiltonian $\hat{H}$. Other interactions cannot be conveniently included in the Hamiltonian description (such as collisions between atoms and spontaneous emission). One way of including these effects is to introduce γ_{nm} and Γ_{nm} that describe the damping of the system.

$$\frac{d\rho_{nm}}{dt} = \frac{i}{\hbar}\left[\hat{\rho}, \hat{H}\right]_{nm} - \gamma_{nm}\rho_{nm}, n \neq m \tag{2.17}$$

$$\frac{d\rho_{nm}}{dt} = \frac{i}{\hbar}\left[\hat{\rho}, \hat{H}\right]_{nm} - \sum_{E_m > E_n} \Gamma_{nm}\rho_{mm} - \sum_{E_m < E_n} \Gamma_{mn}\rho_{nn} \tag{2.18}$$

Here γ_{nm} gives the damping effect of the ρ_{nm} coherence and Γ_{nm} the decay from level m to level n. In general the off-diagonal damping can be represented as

$$\gamma_{nm} = \frac{1}{2}(\Gamma_n + \Gamma_m) + \gamma_{nm}^{col} \tag{2.19}$$

Γ_n and Γ_m are the total decay rates of population out of levels n and m. And γ_{nm}^{col} is the dephasing rate to processes that are not due to population decay.

2.3 Optical Bloch equations for a two-level system

After this short survey of quantum mechanics that is relevant for optical interactions, I will discuss the optical Bloch equation. The *Bloch vector* formalism is a common way to describe the coherent evolution of a quantum state and is used in this report. The Bloch equations are the density matrix equations for a two-level atom (fig 2.1). This proof largely follows the proof given by Boyd [1] expect for some shortcuts.

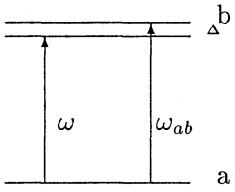

Figure 2.1: Near-resonant excitation of a two-level atom.

The Hamiltonian for this system is $\hat{H} = \hat{H}_0 + \hat{V}(t)$, where $\hat{H}_0$ is the atomic Hamiltonian and $\hat{V}(t)$ is the interaction with the electromagnetic field. Energies of states a and b are written as $E_a = \hbar\omega_a$ and $E_b = \hbar\omega_b$. We assume that the dipole interaction with the electromagnetic field has the form $\hat{V}(t) = -\hat{\mu}\tilde{E}(t)$, where $\hat{\mu}$ is the dipole moment operator of the atom. Further it is assumed that

the states a and b have definite parity so that diagonal elements of $\hat{\mu}$ vanish and then hence $V_{aa} = V_{bb} = 0$. We then get

$$V_{ba} = V_{ab}^* = -\mu_{ba}\tilde{E}(t) \tag{2.20}$$

For a two-level system the density matrix consists of only four components.

$$\hat{\rho} = \begin{bmatrix} \rho_{aa} & \rho_{ab} \\ \rho_{ba} & \rho_{bb} \end{bmatrix} = \begin{bmatrix} c_a c_a^* & c_a c_b^* \\ c_b c_a^* & c_b c_b^* \end{bmatrix} \tag{2.21}$$

Where $\rho_{ba} = \rho_{ab}^*$. By introducing the transition frequency $\omega_{ab} = (E_a - E_b)/\hbar$ we can write the *Liouville equation* as

$$\dot{\rho}_{ab} = -i\omega_{ab}\rho_{ab} - \frac{i}{\hbar}\sum_k (\rho_{kb}V_{bk} - V_{ka}\rho_{ak}) \tag{2.22}$$

Or in a less compact form

$$\dot{\rho}_{ba} = -i\omega_{ba}\rho_{ba} + \frac{i}{\hbar}V_{ba}(\rho_{bb} - \rho_{aa}) \tag{2.23}$$

$$\dot{\rho}_{ab} = -i\omega_{ab}\rho_{ab} + \frac{i}{\hbar}V_{ab}(\rho_{aa} - \rho_{bb}) \tag{2.24}$$

$$\dot{\rho}_{bb} = \frac{-i}{\hbar}(V_{ba}\rho_{ab} - \rho_{ba}V_{ab}) \tag{2.25}$$

$$\dot{\rho}_{aa} = \frac{-i}{\hbar}(V_{ab}\rho_{ba} - \rho_{ab}V_{ba}) \tag{2.26}$$

This is the time evolution for the density matrix for a two-level atom in interaction with an electromagnetic field. Relaxation processes are yet to be added to equations. We do that by adding the decay rate $\Gamma_{ba} = 1/T_1$ from the excited state, where T_1 is the lifetime of the excited state. We also assume that we have loss of coherence, with a characteristic time T_2, leading to the dephasing $1/T_2 = \gamma_{ba}$. Since $\rho_{ab} = \rho_{ba}^*$ no separate equation for ρ_{ab} is needed.

$$\dot{\rho}_{ba} = -(i\omega_{ba} + \gamma_{ba})\rho_{ba} + \frac{i}{\hbar}V_{ba}(\rho_{bb} - \rho_{aa}) \tag{2.27}$$

$$\dot{\rho}_{bb} = -\rho_{bb}\Gamma_{ba} - \frac{i}{\hbar}(V_{ba}\rho_{ab} - \rho_{ba}V_{ab}) \tag{2.28}$$

$$\dot{\rho}_{aa} = \rho_{bb}\Gamma_{ba} - \frac{i}{\hbar}(V_{ab}\rho_{ba} - \rho_{ab}V_{ba}) \tag{2.29}$$

By inspection we see that

$$\dot{\rho}_{bb} + \dot{\rho}_{aa} = 0 \tag{2.30}$$

so

$$\rho_{bb} + \rho_{aa} = 1 \tag{2.31}$$

is a conserved quantity since we are considering a closed two-level system. It is usually more favourable to consider the population difference $\rho_{bb} - \rho_{aa}$ and as one can see (2.27) include that term. By making the variable substitution

$$w(t) = \rho_{bb} - \rho_{aa} \tag{2.32}$$

and using the relation

$$-2\rho_{bb} = -(1 - \rho_{aa}) - \rho_{bb} = (\rho_{aa} - \rho_{bb}) - 1 = -w - 1 \tag{2.33}$$

and subtracting (2.28) and (2.29) from each other we obtain

$$\dot{\rho}_{ba} = -(i\omega_{ba} + \gamma_{ba})\rho_{ba} + \frac{i}{\hbar}V_{ba}w \tag{2.34}$$

$$\dot{w} = -(w + 1)\Gamma_{ab} - \frac{2i}{\hbar}(V_{ba}\rho_{ab} - \rho_{ba}V_{ab}) \tag{2.35}$$

It is common to generalise this equation by introducing population difference at thermal equilibrium w^{eq} that can have another value than -1 as in (2.35). $w(t) = -1$ would mean that all atoms are in their ground state.

Now we turn our attention back to (2.20) that explicitly show how the interaction depend on the electromagnetic field. We assume that we have a monochromatic steady-state field with frequency ω interacting with the system. The interaction Hamiltonian is then given by

$$V_{ba} = V_{ab}^{*} = -\mu_{ba}(Ee^{-i\omega t} + E^{*}e^{i\omega t}) \tag{2.36}$$

The part of V_{ba} that oscillates as $e^{-i\omega t}$ acts as a far more effective driving term than the part that oscillates as $e^{i\omega t}$. This is because ρ_{ba} varies slowly in comparison with the frequency of the optical field. A driving term whose phase changes during an optical cycle will not affect ρ_{ba}, so the $E^{*}e^{2i\omega t}$ part is set to zero. The effective Hamiltonian can then be approximated as

$$V_{ba} = -\mu_{ba}Ee^{-i\omega t} \tag{2.37}$$

This is called the rotating wave approximation (RWA). Inserting the expression for V_{ba} into (2.33) and (2.34) give us

$$\dot{\rho_{ba}} = -(i\omega_{ba} + \gamma_{ba})\rho_{ba} - \frac{i}{\hbar}\mu_{ba}Ee^{-i\omega t}w \tag{2.38}$$

$$\dot{w} = -(w - w^{eq})\Gamma_{ab} + \frac{2i}{\hbar}(\mu_{ba}Ee^{-i\omega t}\rho_{ab} - \mu_{ab}E^{*}e^{i\omega t}\rho_{ba}) \tag{2.39}$$

We now introduce a slowly varying off-diagonal matrix component $\sigma_{ba}(t)$ and define it as

$$\rho_{ba}(t) = \sigma_{ba}(t)e^{-i\omega t} \tag{2.40}$$

By introducing this and the frequency detuning $\Delta = \omega - \omega_{ba}$ equation (2.37) and (2.38) turn into

$$\dot{\sigma_{ba}} = (i\Delta - \gamma_{ba})\sigma_{ba} - \frac{i}{\hbar}\mu_{ba}Ew \tag{2.41}$$

$$\dot{w} = -(w - w^{eq})\Gamma_{ab} + \frac{2i}{\hbar}(\mu_{ba}E\sigma_{ab} - \mu_{ab}E^*\sigma_{ba}) \tag{2.42}$$

We further assume that $\mu_{ge} = \mu_{eg} = \mu$ and choose the phase of the electromagnetic field such that $E = E^*$. An important and commonly used term in quantum optics is the *Rabi frequency*. The classical interpretation of the Rabi frequency is how fast an electromagnetic field can drive an atom between two energy levels. It is introduced here as

$$\Omega = \frac{2\mu E(t)}{\hbar} \tag{2.43}$$

$$\dot{\sigma_{ba}} = (i\Delta - \gamma_{ba})\sigma_{ba} - \frac{i}{2}\Omega w \tag{2.44}$$

$$\dot{w} = -(w - w^{eq})\Gamma_{ab} + i\Omega(\sigma_{ba} - \sigma_{ab}) \tag{2.45}$$

The density matrix elements $\sigma_{ab} = \sigma_{ba}^*$ are now expressed in their real and imaginary parts as

$$\sigma = \frac{1}{2}(u - iv) \tag{2.46}$$

Equation (2.43) is also separated into its real and imaginary parts as

$$\frac{1}{2}\frac{d}{dt}(u - iv) = \frac{1}{2}(i\Delta - \gamma_{ba})(u - iv) - \frac{i}{2}\Omega w \tag{2.47}$$

$$\dot{u} = \Delta v - \gamma_{ba}u \tag{2.48}$$

$$\dot{v} = -\Delta u - \gamma_{ba}u + \Omega w \tag{2.49}$$

$$\dot{w} = -(w - w^{eq})\Gamma_{ab} + i\Omega(\frac{1}{2}(u + iv) - \frac{1}{2}(u - iv)) = -(w - w^{eq})\Gamma_{ab} - \Omega v \tag{2.50}$$

This set of equations (2.48-2.50) are called the optical Bloch equations and describes the interaction of a two-level system with an electromagnetic field.

2.3.1 The Bloch Sphere

It is common to visualise the Bloch equations by describing the atomic population and coherence as a vector in the (u, v, w)-space. The *Bloch vector* (fig 2.2) is defined as $R = (u, v, w)$. We now consider the case without relaxation processes. At equilibrium, $u = v = 0$ and $w = -1$, which gives a constant length of the Bloch vector equal to 1. The Bloch vector can then move within a sphere with radius 1, the *Bloch sphere*.

The projection of R on the w-axis tells us the population difference. The u- and v-axis are related to the phase coherence of the state relative to the phase of the electromagnetic field. The u part is the component in phase with the

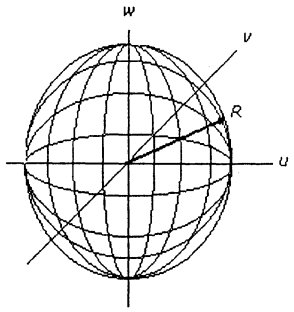

Figure 2.2: Bloch vector diagram

electromagnetic field and v is out of phase. When a field is applied to the system all three components increase, since u and v are cross coupled in the case that we have a frequency detuning $\Delta \neq 0$. When the field is turned off, the loss of coherence in the system causes the u and v components to decrease in length and become zero when we have relaxation. The population decay will relax the system in the $-w$ direction into their thermal equilibrium w^{eq}. As long as the Bloch vector moves on the Bloch sphere all atoms are in a superposition of the two states. When w is equal to zero and $u^2 + v^2 = 1$ the system is in an equal coherent superposition of states.

2.3.2 $\pi/2$- and π-pulses

With the use of Bloch formalism the behaviour of a two-level system can easily be visualised using the Bloch sphere. When a field is tuned in resonance with the transition the Bloch vector rotates on the sphere from $w = -1$ to $w = 1$ with a frequency equal to the Rabi frequency Ω. This is usually called *Rabi flopping*. Other important concepts are π and $\pi/2$ pulses. A π pulse transfers the whole population to the excited state. The Bloch vector is then rotated up to $w = 1$. A $\pi/2$ pulse rotates the Bloch vector to an even superposition of the ground and excited state.

2.3.3 Graphical examples of the time evolution of the Bloch vector

By solving the Bloch equation (2.48-2.50) in MatLab it is possible to simulate the behaviour of the Bloch vector. I've tried to choose parameters that are as close as possible to the real parameters in the laboratory.

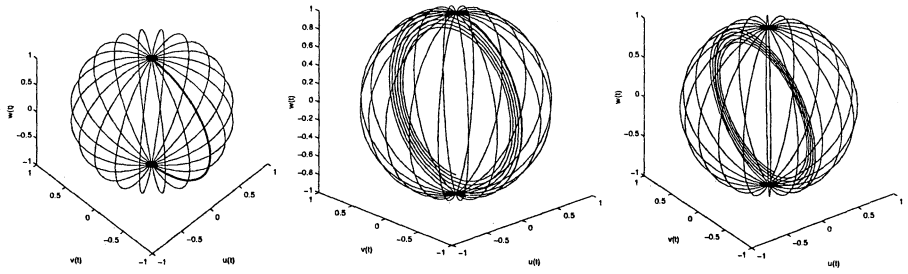

Figure 2.3: The left picture shows a π-pulse, essentially all atoms are brought up to the excited state. The middle figure is Rabi flopping, the Bloch vector rotates with circles on the sphere. The Rabi frequency was 10 MHz in the simulation. Because of relaxation it tend to spiral towards the middle of the sphere. The right figure is Rabi-flopping again, but now for atoms that are detuned from resonance with 100 kHz. Circles are now tilted from the $w(t)$-axis and the *generalised Rabi-frequency* ($\Omega^* = \sqrt{\Omega^2 + \Delta^2}$) now drives atoms between the two states.

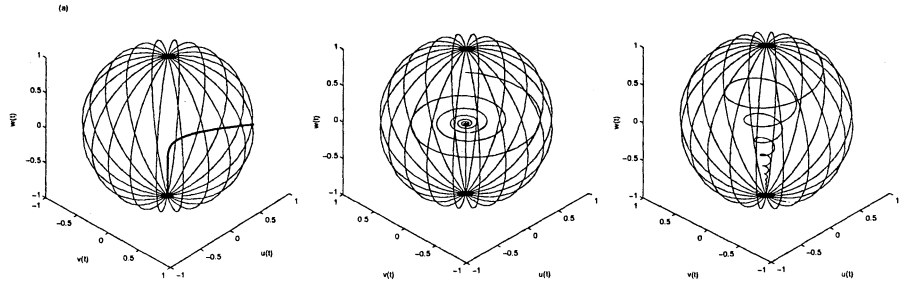

Figure 2.4: These three pictures show the evolution after the electromagnetic field is turned off. The left picture starts as an even superposition and relaxes towards the centre of the sphere quickly and then down to the ground state. This because T_2 is much shorter than T_1, all atoms are on resonance. The middle figure is the same case for atoms out of resonance with each other. The right figure shows a case where atoms start in a state that is near the excited state, out of resonance and $T_1 = 5T_2$.

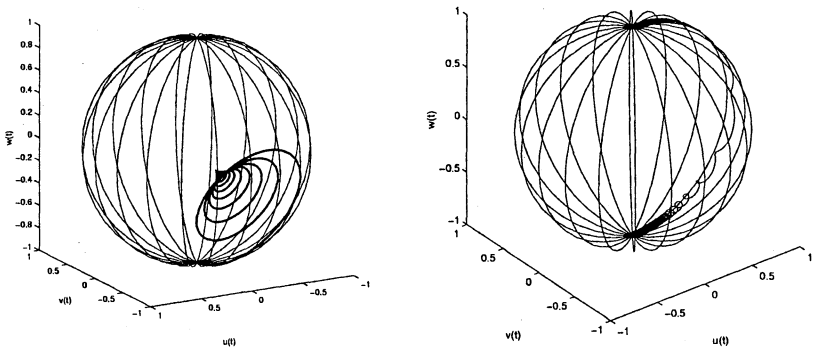

Figure 2.5: The left figure show how atoms out of resonance oscillates with the *generalised Rabi-frequency.* When $t \mapsto \infty$ atoms spirals themselves to the centre of the sphere. It is then 50% chance of emission and 50% chance of absorption, but the state is incoherent. The right figure is an interesting case called *adiabatic following.* The laser is here swept between -20 MHz and 20 MHz when the field is turned on. The Rabi frequency is set to 1 MHz and the chirprate is $0.1MHz/\mu s$. The atoms are still brought up to the excited state, but atoms in a $\approx$ 1 MHz interval essentially feel the same sweep so they also end up in the excited state.

Chapter 3

Coherence

Irreversibility and decay are two prominent phenomena in many-body physics. Several mechanisms can induce decay in a quantum system. But all decay processes need not be irreversible. The discovery in 1950 of *spin echoes* by *E.L. Hahn* [13] showed that free induction decay, in particular, is easily reversed. It is not only easily reversed, but also easily reversed long after the free induction signal has disappeared. The echo signal has the almost magical quality of something coming from nothing. Of course, there is nothing magical about the principles on which echoes are based on and photon echoes have found wide application in the study of coherence decay. The optical analogue of spin echoes were first observed by *Kurnit et al* in 1964 [14].

3.1 Two-pulse echo

The two-pulse echo, also known as *the Hahn echo*, is briefly explained in this section. The experiment is carried out by exciting the sample with two laser pulses separated by a delay τ. The first pulse is ideally a $\pi/2$ pulse that creates a superposition of the ground and excited states. This coherence is detectable because it leads to a macroscopic oscillating dipole. This signal rapidly decays since the individual phase of dipole moments are starting in phase but spread out to a random phase distribution very quickly. Because of their different transition frequencies they accumulate phase differently, which is called free induction decay. The second π pulse has the effect of reversing the sign of the phase accumulation. Thus after an additional time τ, the net phase shift is cancelled for each ion, leading to a rephasing of the original coherence and emission of a burst of coherent radiation. This burst of radiation is called a photon echo. An analogue usually used is that of runners on a track. All runners start together and distribute themselves along the track since they run at different speed. After a time τ they get a signal that they should start running in the opposite direction. Assuming that they run at a constant speed they will return at the same time to the beginning. I want to stress that the two-pulse echo is just one way to create echoes, see [12] or [15] for additional schemes.

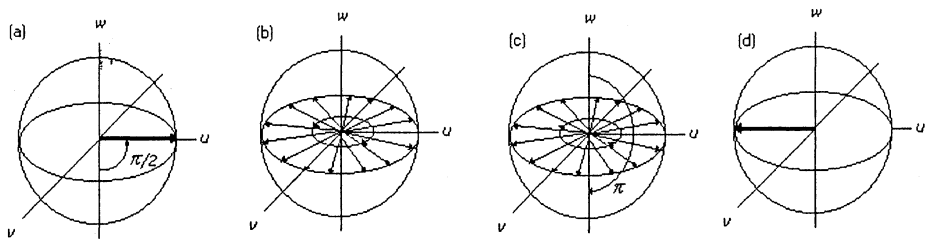

Figure 3.1: Bloch vector diagrams showing how the echo is created. (a) The first $\frac{\pi}{2}$-pulse create an superposition that can be seen as a macroscopic oscillating dipole that is radiating light. (b) The phases of the individual dipoles starts in phase but are then spread out, which causes the free induction decay. (c) A π-pulse after a time τ reverses the sign of the phase accumulation. (d) All atoms get the same phase again after an additional time τ and begin to radiate light.

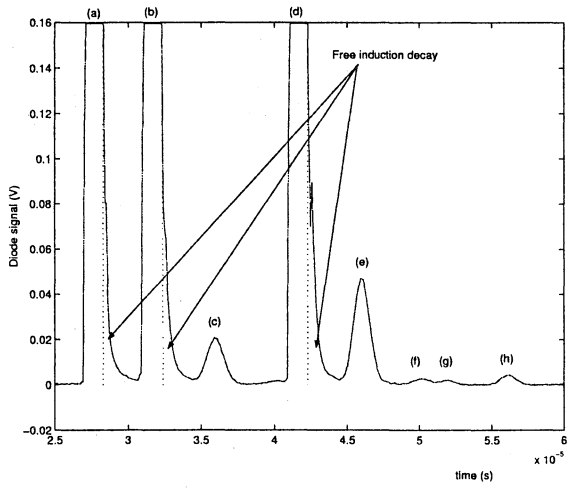

Figure 3.2: Typical photon echo from an experiment. Three pulses (a,b and d) hit the top of the diagram. These are excitation pulses. The first photon echo (c) is a two pulse echo and the last stronger echo is a three-pulse echo (e). Free induction decay can be seen on the right side of excitation pulses. The maximum intensity of a photon echo is usually around 1% of the intensity of excitation pulses. We can vaguely see other two-pulse echoes after the three-pulse echo (f,g and h).

The intensity or amplitude of the echo reflects the decay of coherence due to homogeneous relaxation processes during the time 2τ. The measured signal is the intensity of the echo that give another factor two since $I \propto E^2$. The echo should then decrease as, $I = I_0 e^{-\frac{4t}{T_2}}$. A plot of echo amplitude versus τ give you the coherence time T_2.

Decoherence appears whenever a quantum system is coupled with its environment. Very small perturbations in the environment of the interacting atoms can lead to changes in their transition frequencies and thus lead to dephasing strong enough for detection. The analyses of photon echoes in solids have shown that several dynamical processes can give rise to attenuation of the echo. The most obvious process is that of thermal phonons. This can be avoided by cooling the solid to around 4 K [12]. This leaves effects of the static crystal field and other excited ions as main perturbations for the dopants. The different processes of echo attenuation effects can be summarised as [16]:

$$\Gamma = \Gamma_{LT} + \Gamma_{EQP} + \Gamma_{TLS} + \Gamma_{SI} + \Gamma_{EFS} + \Gamma_{NQP} \tag{3.1}$$

The meaning of the different terms are explained below.

3.2 Thermal equilibrium phonons (EQP)

Thermal equilibrium phonons give a line broadening that is due to increased phonon scattering and phonon absorption. At sufficiently low temperatures there are very few high energy phonons and the effects of EQP become negligible below approximately 4 K. At room temperature however, they can give rise to a line broadening that is of the order 8 magnitudes higher than the line width at 4 K. Optical transition line widths of only 122 Hz has been reported at 2 K in comparison with 60 GHz at room temperature [17].

3.3 Optical decay (LT)

Γ_{LT} represents the lifetime limited value and hence establishes the ultimate limit for Γ. At cryogenic temperatures, the lifetime of excited rare-earth ions in crystals ranges from μs up to ms.

3.4 Lattice two-level system (TLS)

The effects of lattice two-level systems is a weak effect in RE-ion-doped crystals and has only rarely been the subject in the analyses of these systems. But they can give a big contribution in crystals grown under different conditions [18]. In such crystals there exist vibrational modes that are excited by low energy phonons.

3.5 Spin-ion interaction (SI)

Γ_{SI} depends on the dynamics of the host spins that magnetically interact with the dopant ions. The spin-lattice relaxation can usually be slowed down by a

weak permanent magnetic field. Random spin-flips of the neighbouring atoms in the lattice are usually refereed to as *spectral diffusion.* In the search for long coherence times, host material should be chosen such that their elements have zero nuclear spin. The Y_2SiO_5 crystal is then a good choice. Oxygen by having zero nuclear spin, silicon only by the 4.7% abundant ^{29}Si with the nuclear moment -0.56 μ_N and yttrium by having a small magnetic moment -0.14 μ_N [17]. Yttrium substituted by trivalent rare-earth ions further does not require charge compensation. A particular case arises when the dopants have a large enhanced magnetic-dipole moment in the excited state. The lattice spins are then frozen-in close to the dopant. This effect has been discussed in terms of the *frozen-core* model [12] [19].

3.6 Excitation induced frequency shift (EFS)

Instantaneous diffusion or excitation induced frequency shift occur when you excite ions in the sample. The local electrostatic and magnetic environment is modulated by the excitation of neighbouring ions. This induces a nonthermal dephasing that depends on the excitation density. Guest ions mutually interact with each other and they can have different permanent electric dipole moments in their ground and excited state. An excited ion induces a Stark effect in neighbouring ions that lead to dephasing. This model is strongly supported by Stark-modulated photon echoes (SMPE) experiments [20].

3.7 Nonequilibrium phonons (NQP)

Γ_{NQP} accounts for non-equilibrium phonons that are generated by the decay of the electronic excitations. If atoms are decaying by different routes than the normal optical decay they can in the last step relax by sending out nonequilibrium phonons (fig 3.3). The importance of NQP depend on how often they can interact with other ions. A high concentration of ions might trap NQP in the crystal and lead to a dephasing. If the concentration is low it might be unlikely that NQP will interact as they propagate out of the crystal and do not cause any dephasing. According to [16] NQP is likely to occur for Pr^{3+} site I in Y_2SiO_5.

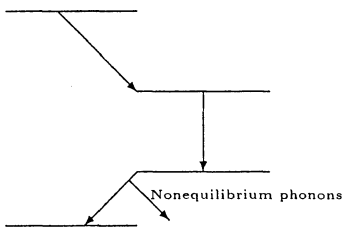

Figure 3.3: Creation of Nonequilibrium phonons (NQP).

Chapter 4

Quantum Computers

4.1 General

The concept of quantum computers is rather new and has been studied extensively the past two decades. The potential power of quantum phenomena that can perform computations was first presented in a talk by Richard Feynman at MIT 1981. He observed that it appeared to be impossible to simulate the evolution of a quantum system on a classical computer in an efficient way. He pointed out that setting up the experiment and measuring the outcome is equivalent to perform very complex computations. The Quantum Turing Machine was first described by David Deutch 1985. Quantum computers open up a whole new field of logic in computers and algorithms because of the consequences that quantum mechanics bring. Even though that we are reaching the limit of performance for classical computers, quantum computers will not be able to compete with them for several decades, if ever. They will rather be a subclass of computers that can do specific tasks where they may outclass classical computers. To find out more about this field read e.g. references [2] and [3].

4.2 The Qubit

Superposition and entanglement are the basic principles upon which quantum computers are based and these principles make a quantum computer different from a classical computer. Qubits are the quantum mechanical counterpart of classical computer bits. A qubit has two states either $|1>$ or $|0>$ but can also be in any superposition of these states.

That states can be in a superposition is not so intuitive. Therefore I will give you an example of an experiment that shows that a photon has to be in a superposition otherwise the experiment would not work. The set-up uses a beam splitter, when a photon hits the beam splitter it is 50% chance that it will get reflected and 50% that it is transmitted. So you can expect the photon

to randomly take one of the paths with equal probability. If we place two detectors that detect the reflected and transmitted photon you register photons with the same probability in both detectors, as you would suspect. However if we recombine the two beams in a second beam splitter before the detectors you can observe fascinating quantum interference phenomena.

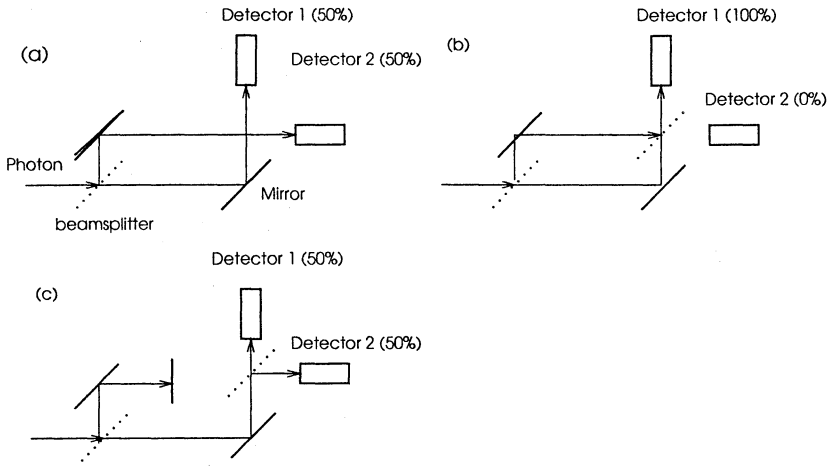

Figure 4.1: Quantum interference experiment. (a) One beam splitter divides the beam into two beams, equal probability to hit detector one and two. (b) Adding an additional beam splitter where the two beams overlap. There are now 100% probability that the photon strikes detector 1. (c) Blocking off one beam and you again get equal probability to strike detector one and two.

If it was 50% chance for the photon to follow either the transmitted or reflected beam from the first beam splitter then we would still register photons with equal probability at both detectors. However that is not how it works. If the two possible paths are exactly equal in length, then it turns out that there is a 100% probability that the photon strikes detector 1. This is because the photon interferes with itself, destructively along one path. It seems inescapable that the photon must have actually travelled both paths at once. If you place a screen in the way of either of the routes, then it again becomes equally probable that detector 1 or 2 is reached. The photon somehow knows that it is not permitted to travel along one path and therefore takes the other path. I know this sounds a bit strange. But this is how nature works, the only universe that we can see is the universe where the interference is strong. All possible universes where photons travel a route where it should not go, can not be observed by us. Well that is how I understand it, other would argue that we are living in a universe that is an infinite parallel universe. You can say that the photon is in a coherent superposition of being the reflected and transmitted beam if you use the quantum mechanical description from chapter two.

4.3 Advantages of quantum computers

A classical 3-bit register can store exactly *one* of eight possible configurations. A 3-qubit register can store *all* eight configurations in a superposition. The capacity for storing quantum information increases exponentially and in general L qubits can simultaneously store up to 2^L numbers. The prepared qubits can then be used as one single input for a function. To accomplish the same task with a classical computer you would have to do the computation 2^L times or have 2^L processors working in parallel. This is called *quantum parallelism.* However if we measure the register's contents, we will see only one of those numbers and only one answer. Quantum computers offer an enormous gain in comparison with classical computers but only for a certain types of computations. [2]

4.3.1 Quantum computer algorithms

The efficiency of an algorithm is measured in terms of the minimum number of operations it has to do to find the right answer. A quantum computer has no advantages compared to normal computers when it comes to doing normal computations. But there are a few schemes that would make use of the quantum parallelism. Shor's algorithm from 1994 [4] is the one that has received most attention. It factorises large integers. In this case the number of computations on a quantum computer would scale cubically with the size of the integer but super-polynomially on a classic computer. Modern commercial and military cryptography uses the fact that factorisation of very large integers into primes can not be done in practice.[1] But factorisation would be possible with a large scale quantum computer. Lov K. Grover published another algorithm in 1996 [5]. It was a fast quantum mechanical search algorithm for an unsorted database. A classical computer would require $N/2$ operations when Grover's algorithm only require $\sqrt{N}$ operations. Grover's algorithm is more general than that though. It uses the fact that you can give a single input of all numbers and by brute force find the element you want. Applications could span cracking DES[2] that essentially requires a search among 2^{56} possible keys to making chess-playing algorithms that test all possible moves. [2]

All proposed algorithms so far do require a lot of qubits and with the current technology it is not possible to create more then 10 or so interacting qubits. And I do not foresee that this will change radically in the following 10 years. The most promising application of a Quantum Turing Machine might be its ability to simulate some other quantum system or itself, just like a Turing Machine can. To simulate a state vector a classical computer need to manipulate 2^n complex numbers and a quantum computer just needs to handle n qubits. This is open up a fascinating area where you can simulate any quantum mechanical system, which would not be feasible with a normal computer.

[1] RSA is the most commonly used algorithm. RSA stands for Rivest, Shamir and Adleman, the developers of the RSA public-key cryptosystem.

[2] DES-Data Encryption Standard. The most commonly used cryptography algorithm to generate secret keys. There has been a constant debate on how safe DES actually is and it has been cracked a few times, see http://www.distributed.net/.

4.4 Qubit logic gates

A qubit state can be represented by

$$|x>=\begin{pmatrix} \alpha|1> \\ \beta|0> \end{pmatrix} \tag{4.1}$$

A phase gate and the Hadamard gate is sufficient to construct any unitary operation on a single qubit. The phase gate ϕ is defined as $|0>\mapsto |0>$ and $|1>\mapsto e^{i\phi}|1>$ or in matrix notation.

$$\phi = \begin{pmatrix} 1 & 0 \\ 0 & e^{i\phi} \end{pmatrix}$$
$$|x>\ \phi \mapsto e^{ix\phi}|x> \tag{4.2}$$

The Hadamard gate is the most common quantum gate and is defined as,

$$H = \frac{1}{\sqrt{2}}\begin{pmatrix} 1 & 1 \\ 1 & -1 \end{pmatrix}$$

$$|x>\ H \mapsto \frac{1}{\sqrt{2}}((-1)^x|x> +|1-x>) \tag{4.3}$$

The Hadamard gate can be used to create an equal superposition of a single state qubit i.e. ,

$$|0>\ H \mapsto \frac{|0>+|1>}{\sqrt{2}}$$
$$|1>\ H \mapsto \frac{|0>-|1>}{\sqrt{2}} \tag{4.4}$$

The Hadamard gate and the phase gate can be used to transform any input register into any arbitrary superposition of $|0>$ and $|1>$ for all qubits in the register. In general, a register of size $n > 1$ can be prepared in states which are not separable, known as entangled states. To entangle two qubits we have to introduce two-qubit gates. One of the simplest nontrivial operation that would be required to do all quantum logic between qubits would be a quantum controlled-NOT operation [6]. The classical controlled-NOT operation is a reversible logic gate operating on two bits ϵ_c and ϵ_t, where ϵ_c is the control bit and ϵ_t the target bit. The value of ϵ_t is negated if $\epsilon_c = 1$ otherwise it is left unchanged.

$$C_{NOT} = \begin{pmatrix} 1 & 0 & 0 & 0 \\ 0 & 1 & 0 & 0 \\ 0 & 0 & 0 & 1 \\ 0 & 0 & 1 & 0 \end{pmatrix} \begin{pmatrix} \alpha_c\alpha_t|00> \\ \alpha_c\beta_t|01> \\ \beta_c\alpha_t|10> \\ \beta_c\beta_t|11> \end{pmatrix} = \begin{pmatrix} \alpha_c\alpha_t|00> \\ \alpha_c\beta_t|01> \\ \beta_c\beta_t|10> \\ \beta_c\alpha_t|11> \end{pmatrix} \tag{4.5}$$

If the control qubit is in a superposition $\alpha|0> +\beta|1>$ and the target bit is in its $|0>$ state then the C-NOT generates the entangled state,

$$(\alpha|0> +\beta|1>)|0> \xrightarrow{C_{NOT}} \alpha|00> +\beta|11> \tag{4.6}$$

The Hadamard gate, all phase gates and the C-NOT form an infinite *universal set of gates.*

Each quantum logic gate performed on the qubits will cause noise in the system and therefore make them hard to implement, but the discovery of *Quantum Error Correction* [7] has shown that you can reduce the noise in the system without collapsing its state.

4.5 Quantum computer concepts

Several different techniques on how to create a qubit have been proposed the last decade but the constraints on the system are rather harsh and not so easy to fulfil. It must be easy to prepare and detect the quantum states of the qubit. You must be able to create true entangled states and have very low decoherence in the system. The system should also be scalable to a large number of qubits. NMR, ion traps, high-Q optical cavities, quantum dots are some candidates considered as quantum computer hardware. As well as the rare-earth-ion-doped crystals that this thesis explores.

4.5.1 The NMR Quantum Computer

This is the technique that have received most interest from the public and the one that has showed the best results so far. The qubit consists of the two spin-$\frac{1}{2}$ states of a nucleus. The nucleus most commonly used is a hydrogen nucleus (proton). The proton resonance frequency is slightly dependent on the position of the hydrogen atom in the molecule. The two spin states are usually degenerate, but with use of a strong magnetic field the degeneracy can be broken [9]. When a spin transition is done for one state the other protons in the molecule experience a slightly different electromagnetic surrounding and shift their absorption frequency. That is used to couple the different protons to each other. Typically you can use a macro molecule with N protons, where all of them would have a specific absorption frequency. This would make it possible to create a N-qubit system. But fact remains that the signal decrease exponentially with the number of qubits and therefore it might not be possible to scale it beyond 10-15 qubits [8]. To find out more read [3] and [2].

4.5.2 Ion traps

The ion trap consists of an electric field where the ions are trapped by a restoring force in opposite direction of all movements. The ions are cooled down with laser-cooling to prevent thermal vibrations that would change their quantum states [9]. A laser that can be directed to any individual ion is used to manipulate ions. The qubit states used are the ground state $|0>$ and a metastable excited state $|1>$. The ions interact with each other through coupled vibrations [3].

4.5.3 High-Q optical cavities

A high-Q optical cavity is a cavity that can be used to trap one single photon. The proposed qubit state would then be vacuum in the cavity, $|0>$, or a photon in it, $|1>$. The implementation of quantum gates is achieved by sending off-resonant two-level atoms through the cavities and making them mutually interact. From a general point of view, this is analogous to the linear ion trap scheme, except that now the high-Q cavities play the role of the ions, and the atoms play the role of the laser. This makes this *optical case* very interesting since no cooling would be needed [8].

4.5.4 Quantum dots

A quantum dot could be an electron trapped in a potential well in three dimensions. The electron can have discrete energy values within the well and the ground state is used as $|0>$ and a metastable excited state is used as $|1>$. A basic system would have several quantum dots separated by a small distance r. Interaction would be achieved by using the small frequency shift that the different dipole moments of $|0>$ and $|1>$ induces in neighbouring quantum dots [6]

4.5.5 The Silicon quantum computer

The microelectronics industry has decades of experience of controlling the properties and structure of silicon. This will give a silicon-based quantum computer scheme a head start over other schemes when it comes to putting a quantum computer together. The device proposed by Ladd [10] and colleagues suggest that you use ^{29}Si nuclear $\frac{1}{2}$-spins arranged as chains in a $^{28,30}Si$ (spin-0) matrix as qubits. The readout is to be performed by using magnetic resonance force microscopy on an ensemble.

4.5.6 Rare-earth-ions

Rare-earth-ions doped into an inorganic crystal got, at liquid helium temperatures, all requirements that would make a quantum computer feasible. When the RE-ions are doped into the crystal the crystal structure is slightly disturbed and this leads to an inhomogeneous broadening of the RE-ions $4f^n - 4f^n$ absorption frequencies. This inhomogeneous broadening is of the order of several GHz. Homogeneous broadening is experienced equally by all RE-ions in the crystal and is mostly due to the natural broadening caused by the limited lifetime. But lattice phonons, fluctuating nuclear and electron spins also contribute. At liquid helium temperatures the contribution of thermally induced phonons usually is negligible. The homogeneous broadening is then of the order kHz [12]. This have made them suitable candidates for storage materials as the number of bits that can be addressed in a single spatial position can exceed 10^6 in some materials. The reason for narrow homogeneous line width is the fact that f-electrons are shielded by the crystalline environment by the outer $5s$ and $5p$ electrons and are just mildly perturbed by the effects of static crystal field strain. The fact that they are shielded also give them the property of very long homogeneous dephasing time or good quantum coherence. The qubit in this case would consist of two hyperfine levels in the ground state. The hyperfine levels can have hour long lifetimes and ms decoherence times which is more then enough to complete several computations. The controlled logic between qubits is accomplished using the change in permanent dipole moment induced by an optical transition between the ground and excited state of the ions. The change in dipole moment induces a shift in neighbouring qubits that are shifted out of resonance. The combination of GHz inhomogeneous broadening and kHz homogeneous line width would yield about 10^6 individual frequency channels that could be used as qubits, making this a promising scalable quantum computer scheme in a solid state system [11].

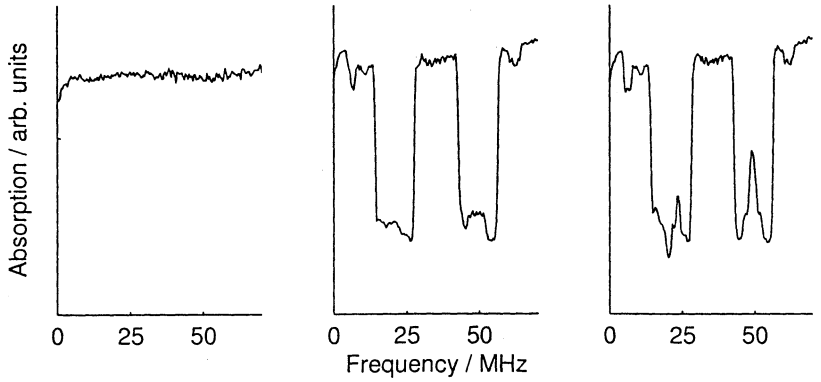

Figure 4.2: A first attempt to construct a qubit. Taken from Tomas Christiansson's Master Thesis [21]. The left picture shows the spectrum before the pumping process, the middle picture is taken after the initial pumping and the right picture is the finished qubit.

Chapter 5

The Pr^{3+} Quantum computer scheme

As already discussed in chapter 3, rare-earth-ion doped inorganic crystals are potential candidates for a quantum computer. I will discuss the scheme based on a Pr:Y_2SiO_5 crystal more in detail in this chapter.

5.1 Praseodymium

Praseodymium can be found with other lanthanide (rare-earth metals) elements in a variety of minerals, but the three principal commercial sources of most of these elements are xenotime, monazite, and bastnaesite [35]. Praseodymium was first separated from the 'rare earth' didymia by Baron Auer von Welsbach in 1885 in Vienna, Austria. Praseodymium is a soft, silvery metal with low toxicity. Its atomic number is 59 and has an atomic mass of 140.91 u. There is just one natural isotope. The atomic radius is 258 pm and its ground state is $^4I_{9/2}$.

K	L		M			N				O		P
s	s	p	s	p	d	s	p	d	f	s	p	s
2	2	6	2	6	10	2	6	10	**3**	2	6	2

Table 5.1: Electron configuration of Pr as free atoms.

When *Pr* is doped into the crystal the two outer *s*-electrons and one of the *f*-electrons bind to the crystal resulting in Pr^{3+} ions. The ground state now becomes $^3H_4$.

K	L		M			N				O		P
s	s	p	s	p	d	s	p	d	f	s	p	s
2	2	6	2	6	10	2	6	10	**2**	2	6	0

Table 5.2: Electron configuration of Pr^{3+}.

5.2 The Y_2SiO_5 crystal

Y_2SiO_5 is a monoclinic biaxial crystal and belong to the C_{2h}^6 space group with eight molecules per unit cell. The lattice parameters are: $a = 1.042$ nm, $b = 0.6721$ nm, $c = 1.249$ nm and $\beta = 102°39'$. The indices of refraction are: $n_a = 1.772$, $n_b = 1.773$ and $n_c = 1.793$. Triply ionised rare-earth ions substitute for the Y^{3+} ions and occupy two inequivalent crystallographic sites with no rotational point symmetry (C_1). [21] [22] The crystal I have been working with had a dopant concentration of 0.05% Praseodymium.

5.3 The Absorption profile

Quantum numbers are generally based on symmetric properties and good quantum numbers require appropriate symmetries. The crystal has low-symmetry and the crystal field quenches the orbital angular momentum (J, L and S) and first-order hyperfine interactions are then forbidden. The only naturally occuring isotope of *praseodymium* has a nuclear spin of $\frac{5}{2}$. The electronic singlet states are then split by the crystal field into three Kramer doublets. Due to the low site symmetry the nuclear wave functions are assumed to be mixed causing the $\Delta m_I = 0$ selection rule to break down [23]. When the Pr^{3+}-ions substitute for Y^{3+}-ions they will distort the crystal structure and this lead to an inhomogeneous broadening of the Pr^{3+}-ions absorption line. The inhomogeneous width is of the order of GHz and the homogeneous line width only of the order of kHz.

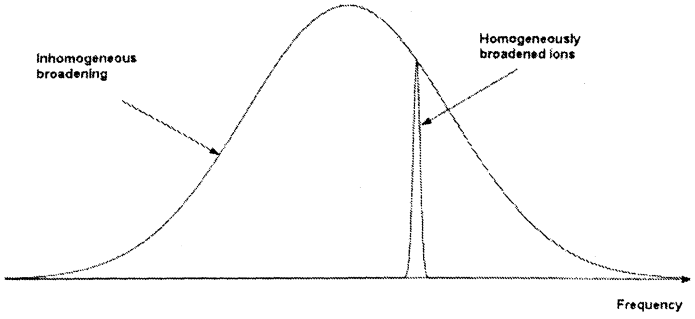

Figure 5.1: Inhomogeneous and homogeneous line widths.

The sharp spectral lines are due to the fact that the f-electrons are shielded from the crystalline environment by the outer $5s$ and $5p$ electrons. The crystal field is however different at the two sites in the crystal. This leads to different absorption frequencies for the two sites.

Parameters	*Pr site I*	*Pr site II*	Reference
λ_0 (air) (nm)	605.813	607.770	[16]
Γ_{LT} (Hz)	970 ± 30	720 ± 16	[22]
Γ_{inh} (GHz)	4.4	2.5	[22]
α (cm^{-1})	10	1.3	[22]
T_1 (optical) (μs)	164 ± 5	222 ± 5	[22] [16]
T_2 (optical) (μs)	111 ± 5	306 ± 5	[22] [16]
f	3×10^{-7}	3×10^{-8}	[16]
$\Delta\mu$	7.3×10^{-2}	6.0×10^{-2}	[16]

Table 5.3: Spectroscopic data taken from articles. Note that the data is from different crystals with different concentration and different geometry. The data depend strongly on the dopant concentration. The oscillator strength (f) and wavelength (λ_0) is the same for all Pr:Y_2SO_5 crystals. Γ_{LT} is the homogeneous line width and Γ_{inh} is the inhomogeneous line width. T_1 is the lifetime of the excited state and T_2 is the coherence time for the optical transition . α is the absorption coefficient and $\Delta\mu$ the difference between the electric dipole moment in the excited state and in the ground state.

The inhomogeneous broadening is almost twice as big for site I then for site II and the oscillator strength (f) is ten times bigger. Thus from the table it is clear that we rather use site I then site II.

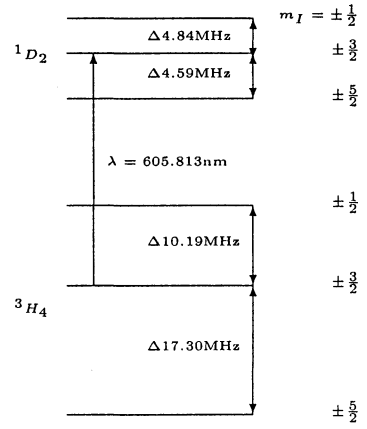

Figure 5.2: Energy level diagram of Pr:Y_2SiO_5 (Site 1) [22] [16].

5.4 Qubit construction

The qubit is chosen to be two of the ground state hyperfine levels. The remaining hyperfine level is used as a reservoir state. Qubits are created within the inhomogeneously broadened optical transition and addressed by tuning the laser. To get a well defined quantum state you optical pump ions to only one

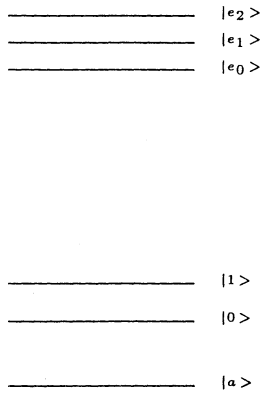

Figure 5.3: Energy level diagram showing the two qubits states.

hyperfine level. This is done by continuously pumping from two of the ground state hyperfine levels to an excited state. If this is done for several excited state lifetimes, the whole population will end up in the third hyperfine level. Ions that did not absorb at both of those frequencies will be pumped away to hyperfine levels where they no longer interact in this step. As the hyperfine level lifetime is very long it is straight forward to perform efficient pumping. The lifetime of the hyperfine level ranges seconds without a magnetic field to minutes or even hours if you apply a magnetic field. One-qubit operations, such as population transfer between the qubit states, can then be performed using *Raman* transitions via the excited state. In theory it seems to quite easy to manipulate the ions but we run into a lot of technical problems at this stage.

Each ensemble of ions that make a qubit must absorb at the same frequency if we want to manipulate them using for instance a π-pulse. Wide enough spectral holes are burnt around the states of the qubit in order to make the whole qubit experience the same pulse area, usually refereed to as a hard optical pulse [24]. The spectral and spatial intensity profile of the laser beam over the qubit must be the same for all ions. High spectral intensity is achieved by using as short pulses as possible. You also need to create a top hat profile of the spatial intensity. This can be done if you use different beam diameters for different steps in the qubit construction [21].

When two spectral holes are burned around the $|0>$ and $|1>$ states ions end up in the third $|a>$ state. Using Raman pulses you can now transfer these back to a superposition of $|0>$ and $|1>$.

5.5 Qubit interaction

Qubit interaction can be accomplished by using the fact that Pr^{3+} has different permanent electric dipole moment in the ground state μ_g and the excited state μ_e. The electric field around the ion is then changed when it is excited and this lead to a change of the absorption frequency for all ions close enough in space. The shift depends on the distance between the ions i and j as [11]:

$$\Delta_v = \frac{(\delta\mu)^2}{4\pi\epsilon_0\epsilon h r_{ij}^3}(\hat{\mu_i}\hat{\mu_j} - 3(\hat{\mu_i}\hat{r})(\hat{\mu_j}\hat{r})) \tag{5.1}$$

where r_{ij} is the distance between ions i and j, h is *Planck's constant* and ϵ_0 is the permittivity of free space. $\hat{\mu}$ and $\hat{r}$ are unit vectors along $(\hat{\mu_e} - \hat{\mu_g})$ and $(\hat{r_i} - \hat{r_j})$. The difference in dipole moment becomes $\delta\mu = \frac{(\hat{\mu_e} - \hat{\mu_g})E}{|E|}$. One excited ion will shift the absorption frequency of the neighbouring ions by about 1 GHz, 1 MHz and 1 kHz for distances r_{ij} equal to 1 nm, 10 nm and 100 nm. Even if the calculations are a bit more complicated than this, we only have to say that we will use ions that interact strongly enough i.e. change each other's frequency enough that they are no longer in resonance with the laser pulses. Ions that are not shifted out of resonance have to be moved to the $|a>$ state. The dipole moments are the same for all hyperfine levels of a given electronic state.

The ions that will make two mutually interacting qubits can then be selected in this way.

1. Select two frequency channels that are going to be used as qubits, $|1>_i$ and $|1>_j$. We consider them being in their $|1>$ states. The two qubits are distinguished by their subscript.
2. We now only want ions that can be shifted by ion-ion interaction. A π-pulse is then applied to $|1>_i$, this shift some of the $|1>_j$ ions out of resonance. The remaining $|1>_j$ ions in resonance are optically pumped to the $|a>_j$ state.
3. Another π-pulse transfers i-ions back to their $|1>_i$ state. Shifted j-ions will now return to their original absorption frequency.
4. The procedure is repeated. But now we let j-ions shift the i-ions out of frequency and remove the unwanted i-ions.
5. The two qubits can now mutually interact by putting either of them into their excited states.

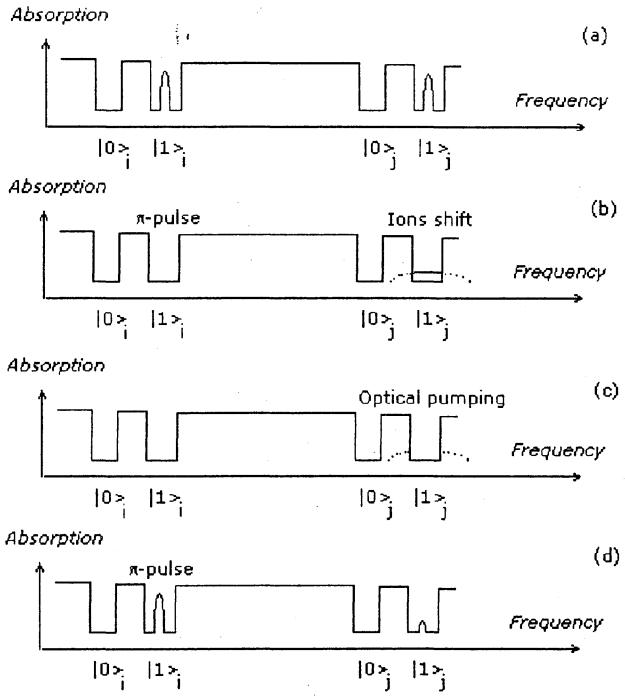

Figure 5.4: (a) Both qubits before the refining procedure. (b) The qubits after a π-pulse has transferred i-ions to the excited state. The j-ions are shifted in frequency by ion-ion interaction. (c) Optically pumping of j-ions that have not shifted enough. (d) Transferring back i-ions from their excited state. Note that the absorption spectrum is simplified. Increased absorption at the $|a>$ frequency and other ions that have been pumped away are not shown.

5.6 C-NOT operation

With use of two interacting qubits it is now possible to create a control-NOT gate. Consider c to be the control qubit and t to be the target qubit. Both qubits can be in any superposition of their $|1>$ and $|0>$ states. If the control qubit is in its $|0>$ state then nothing should happen to the target qubit. The following scheme perform a control-NOT on the two qubits.

1. π-pulse on $|0>_c$ - $|e>_c$
2. π-pulse on $|0>_t$ - $|e>_t$
3. π-pulse on $|1>_t$ - $|e>_t$
4. π-pulse on $|0>_t$ - $|e>_t$
5. π-pulse on $|0>_c$ - $|e>_c$

If the controlling qubit is in its $|0>$ state the target qubit will be shifted out of resonance by ion-ion interaction after step 1. Step 2 to 4 will not change the state of the target qubit then. Step 5 deexcites the control qubit.

However if the controlling qubit is in its $|1>$ state the target qubit will remain unshifted. If the target bit was in its $|0>$ state step 2 and 3 will put it in its $|1>$ state. Step 3 and 4 puts the target bit originally in its $|1>$ state in its $|0>$ state. The control qubit and target qubit will in the general case be in a superposition of their two states. The control-NOT gate then put these qubits in an entangled state. The scheme can be generalised to create multi-qubit control-NOT gate by repeating the first and last step for all control qubits.

5.6.1 The Qubit-bus

Moelmer's group in Aarhus has proposed an architecture [37] where you use one qubit as a data-bus. All gate operations should then go via this particular qubit. The advantage is that you only need to ensure interaction between the qubits and the bus and not between any pair of qubits. The qubit-bus could consist of ions of the same kind as ions in other qubits, but it might as well consist of a different kind of ions that has good interaction properties but it would not require as good coherence as data qubits. If you use the same ions in both qubits and the qubit-bus you can look for transitions where the difference in the electric dipole moment is large for the qubit-bus.

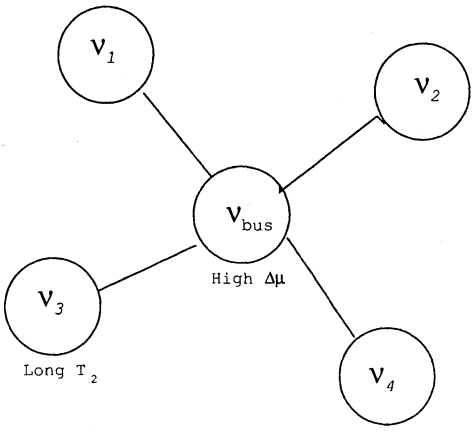

Figure 5.5: Four qubits are coupled to the qubit-bus but not to each other.

Chapter 6

Equipment

6.1 The CR699-21 dye laser system

Experiments were conducted with a *Coherent CR-699-21* ring dye laser, pumped by a *Coherent* Ar^+-ion laser. The dye was *Rhodamine 6G* that make the dye laser tuneable from around 570 nm to 640 nm [9]. The Argon-laser had an output of around 7-8 W which yielded a maximum single-mode power of around 250 mW around 605.8 nm that was the wavelength used in all experiments. The wavelength was measured with the use of a wavelength meter [32].

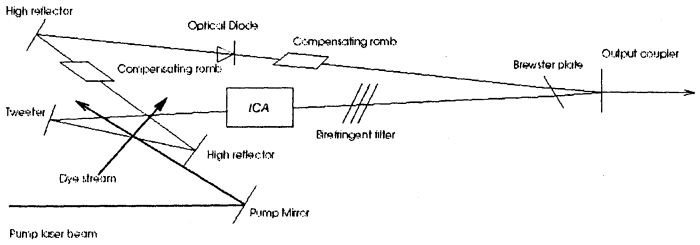

Figure 6.1: Schematic mirror set-up in the dye laser. ICA stands for intracavity assembly and has one thick and one thin etalon.

6.1.1 Single frequency operation

Three optical elements are used to achieve single frequency operation. A *Lyot filter*, a thin etalon and a piezoelectrically driven thick etalon. When tuning the laser over larger frequencies the Lyot filter mounted at Brewster's angle is used. The dominant transmission maximum of this filter can be moved by turning the optical axis of the filter with respect to the plane of polarisation of the light

in the cavity. This results in a bandwidth of about 0.3 Å [9]. This permits several hundreds of modes to lase. The thin and the thick etalon are then used to choose only one single mode among these. This gives the laser a line width of 1 MHz or a coherence for about 1 μs. [25]

6.1.2 Frequency locking

The dye laser frequency is locked to a temperature stabilised *Fabry Pérot* reference cavity. The reference cavity has a transmission, which varies repetitively with optical frequency. The reference signal (A) is set such that it corresponds to the intensity transmitted half way up a cavity transmission peak. A deviation in laser optical frequency causes a change in the transmission signal (B). Signals A and B are subtracted to produce the error signal that is used in a servo-loop to produce a lock-point. The servo-loop adjusts the dye laser cavity length by driving a high-frequency piezoelectric mounted folding mirror (tweeter) and by tilting a Brewster plate. The long term frequency stability for the dye laser is about 30 MHz/hour [25] which is caused by the thermal drift of the reference cavity.

6.1.3 Frequency tuning and scanning

To scan a single frequency, the effective cavity length must be changed. An increase in length moves the output to a lower frequency. A decrease obviously has the opposite effect. The Brewster plate is used to vary the length. To scan in locked single mode, the frequency of the reference cavity is varied. This is accomplished by tilting an additional Brewster plate which is situated inside the reference cavity. As the reference frequency changes, the stabilisation causes the laser to track this frequency, maintaining the narrow line width during a locked-scan. Scans of up to 30 GHz can be made in locked mode [25].

6.2 The Cryostat

The crystal is placed in a chamber that can be filled with liquid helium. High vacuum surrounds the chamber to avoid heat transfer. Further the high vacuum is surrounded by liquid nitrogen that in turn is surrounded by another layer of high vacuum. Two entrances give optical access to the crystal sample, each having three layers of glass. A 4% reflection at each window is expected, giving a total of 12 reflections in glass surfaces of the cryostat. You also get two additional reflexes from the crystal. This gives us a total reflection loss of approximately 56%. The sample is put on a crystal holder that can rotate the sample around the optical axis. The cryostat holds about 10 litres of liquid helium. This is enough for 40 hours of experiments before it needs to be refilled. This construction enables operation at temperatures around 4 K. A vacuum pump is connected to the system, which make it possible to lower the pressure and thus the temperature further to below 2 K.

6.3 Acousto-optic modulators

Several acousto-optic modulators (AOMs) are used in the experiments. They are used for frequency modulation, intensity control and as fast optical shutters. The theory of AOMs is quite simple. A crystal changes its refractive index due to mechanical stress [26]. Acoustic waves are generated in the crystal by a piezoelectric transducer that is driven by a RF signal source. The acoustic wave is perpendicular to the incoming laser beam and due to the spatially periodic density variations in the crystal the light experiences a grating. The acoustically generated travelling waves of index of refraction diffracts the incident light as the atomic planes of a crystal diffracts x-rays in Bragg scattering [1]. With an aperture it is possible to choose just the $1st$ or $-1st$ order of the light. No light will then be diffracted in the corresponding direction when the AOM is turned off. This is essentially a very fast optical shutter, which we use to create laser pulses.

Another important property is that the acousto-optic modulator also causes a frequency shift. The crystal lattice is moving at a velocity equal to the velocity of the acoustic wave. This leads to a Doppler shift of the frequency for the diffracted beams. This can be either positive or negative depending on whether the diffraction order is deflected towards or away from the propagation direction of the acoustic wave. Another way to see this is to consider the scattering of an optical photon with momentum $\hbar k$ and energy $\hbar\omega$ from m acoustic phonons each with momentum $\hbar k_s$ and energy $\hbar\omega_s$, where ω_s is the angular frequency of the acoustic wave. The conservation of energy and momentum gives us the frequency shift.

$$\Delta v = m\omega_s \tag{6.1}$$

The AOMs have a voltage controlled frequency oscillator that typically gives 3.3 MHz/V when the voltage is varied for the AOM RF source.

The AOM is opened when 5 V is applied across a gate. However it can be opened partially by applying ≈ 1 V or more. The transfer function is non-linear and it need to be experimentally determined for each AOM. In my case it was sufficient to know that they did not let too much light through.

6.4 Detection

Strong optical signals can be detected with photodiodes. Small signals have to be detected by a photomultiplier tube.

6.4.1 The Photodiode

Two identical Hamamatsu, $S1223$ PIN-photodiodes were used. They were built in a module together with an amplification stage and a bias battery. The diode is faster when you use it in bias mode and then have a cut-off frequency of 30 MHz. The bias mode gives a higher noise level.

6.4.2 Photomultipliers

Photomultiplier tubes (PMT) are extremely sensitive light detectors. The ability to detect single photons gives the PMT large advantages over other light detectors. A Thorn, 9816QB PMT was used in some experiments. To avoid exposure to strong laser pulses, that would damage the PMT, an AOM was used as a gate that is only opened during the measurement.

6.5 Electronics

6.5.1 Pulse generators

Several different pulse generators were used during the experiment and in several different configurations. They were used to control AOMs, trigger the oscilloscope and to control each other.

- Stanford Research System, *SRS DG535* Four-channel digital delay/pulse generator
- Stanford Research Systems, *SRS DS345* 30 MHz digital arbitrary waveform generator.
- Stanford Research Systems, *DG135*. Four $DG135$ cards was used and controlled by a computer. Each $DG135$ has its own $T0$ output and two delay channels, A and B. $T0$ can be used as initial trigger for other systems and A and B can be used to create pulses.
- *Hewlett Packard 8013B* pulse generator. Delay pulse generator
- *Hewlett Packard 8003A* pulse generator. Pulse generator
- *TTi TGA1244* Arbitrary Waveform generator. Four-channel 40 MHz digital arbitrary waveform generator.

6.5.2 The Oscilloscope

All the data was gathered with the same oscilloscope. The oscilloscope was connected to a computer to which you could transfer oscilloscope data.

- Tektronix, *TDS540* four-channel digital 1 Gs/s oscilloscope.

Chapter 7

Spin-coherence excitation using time delayed Raman pulses

A first attempt to measure the coherence between the two hyperfine splittings in the ground state was done using photon-echoes, not an ordinary three-pulse echo but a slightly modified set-up. The objective is to measure the coherence between two hyperfine levels and an ordinary echo would require this to be done in the rf-regime. Our group is more familiar with obtaining signals from the optical transition so I used a scheme proposed by Babbitt [15]. Optical signals also have a much higher quantum efficiency than rf-signals. In the attempt to create a coherent superposition between the two hyperfine levels I first applied a $\frac{\pi}{2}$-pulse on one frequency to create an equal superposition between hyperfine level $|1>$ (fig 7.1) and an excited state. The ions then accumulate phase for a time τ in the optically excited state. A π-pulse with a frequency shift equal to the separation between the hyperfine levels brings down the amplitude from the $|e>$ state to the $|0>$ state. This creates a coherent superposition between $|1>$ and $|0>$. After a time T, that can be varied, a π-pulse on the original frequency excites ions again and it is assumed that an echo will be emitted after a time approximately equal to τ since the ions rephase on the optical transition. They also lose coherence while in the excited state so τ must be chosen to be much smaller than T_2 for the optical transition This loss of coherence does not matter if τ is kept fixed.

However, since there is an inhomogeneous broadening for the hyperfine levels it is not clear that we would get a signal. The inhomogeneous spin broadening is only about 29 kHz [27]. The laser has a line width of 1 MHz, which means that we only excite 0.25% of the optical inhomogeneous line width. If the inhomogeneous broadenings are correlated we would only deal with hyperfine levels that are inhomogeneously broadened by 7 Hz. To calculate the expected time delay of the echo you have to consider how much phase the wavefunction acquires in different parts of the pulse sequence. While in the excited state the

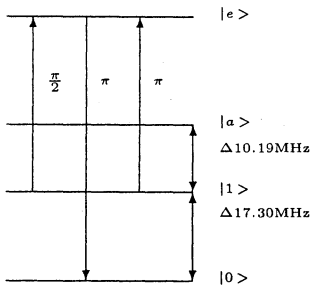

Figure 7.1: Energy level diagram. The excited state is split into 3 levels, but only shown here as one to simplify the discussion.

maximum phase gain is $10^6\tau$ and when they are in a superposition between $|1>$ and $|0>$ the maximum phase accumulation would be $7T$. The net phase to accumulate after the last π-pulse is then $10^6\tau - 7T$, which would give an echo after $\tau - \frac{7T}{10^6}$.

The total delay would then be:

$$\tau^* = \tau - \frac{7T}{10^6} \tag{7.1}$$

The delay of the echo is of no importance if the coherence loss during the rephasing is negligible when T is varied. The small extra time delay because of the inhomogeneous spin broadening will be hard to detect since we do not have detectors that are fast enough. Considering that τ will be in the order of 100 ns and T around 1 ms. That would give an echo after 107 ns instead of 100 ns. So you would need a detector with ns resolution to see the small shift and that is about the limit of our detectors.

That the inhomogeneous spin broadening and the optical inhomogeneous broadening are not correlated was confirmed by *Mitsunaga* [31] in $Eu^{3+} : YAlO_3$. The hyperfine splittings differ by about 10 kHz/GHz for the optical transition. It is not clear what *Ham et al* [27] means with their stated inhomogeneous spin broadening. Numbers agree if you assume that we have a 4 GHz inhomogeneous optical broadening that would give an inhomogeneous spin broadening of about 40 kHz approximately.

7.1 Experimental set-up

In the experimental set-up (fig 7.2) I used two AOMs in series to shift the frequency and create pulses. The 1^{st} order diffracted light was used after each AOM. Three pulses were created with three Stanford Research System $DG135$ cards and they also triggered a HP8013B pulse generator that shifted the frequency of the second pulse. A fourth $DG135$ card controlled the AOM in front of the PMT when this was used as the detector. The output power from the

laser was around 150 mW with 50% loss in the AOMs and 50% loss in the cryostat. Pulse lengths were adjusted to give maximum signal. A lens with a focal length of 10 cm was placed before the cryostat and adjusted to give maximum signal. The signal was either detected by a Hamamatsu, $S1223$ diode or a PMT.

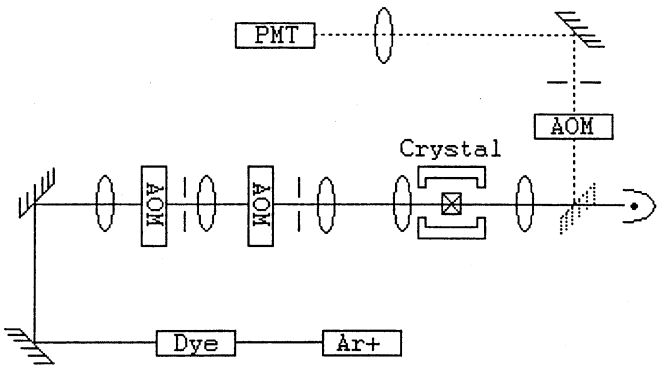

Figure 7.2: An Ar^+-ion laser pumps a dye laser, tuned to 605.813 nm. The light is diffracted in two AOMs that are used to create pulses and shift the frequency. A lens with a 10 cm focal length focuses the light on the crystal. A second lens after the cryostat is used to focus on either a photo-diode or on the third AOM that is used as gate for the PMT.

The following pulse sequence (fig 7.3) was applied when the laser was scanning slowly, 1 GHz every 12 seconds. The repetition rate for the pulse sequence was 20 Hz.

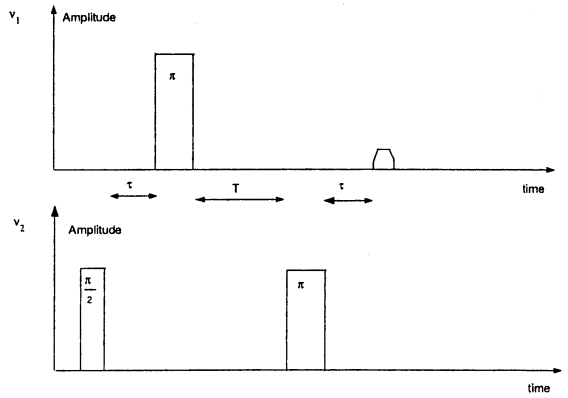

Figure 7.3: Pulse sequence for generating spin-coherence and detecting it using the optical transition. Three laser pulses are used on two different frequencies, ν_1 corresponding to the $|0> -|e>$ transition and ν_2 corresponding to the $|1> -|e>$ transition. Ideally the first pulse pulse on ν_2 should be a $\frac{\pi}{2}$-pulse and the two other pulses should be π-pulses. The echo is supposed to be emitted τ seconds after the last pulse if the time separation between the two first pulses is τ.

7.2 Results

The first part of the experiment was to try to find the signal I was looking for. This was done by changing the frequency of the second pulse. If the frequency of the second pulse does not match the hyperfine splitting in the ground state or the hyperfine splitting in the excited state you should not be able to get a three-pulse echo after the third pulse, since the three pulses would not be interacting with the same ions. This resonance experiment was done with a 4 μs separation between the first and the second pulse and then a 20 μs delay to the third pulse. All three pulses were 500 ns long and the first pulse had a lower amplitude to make it a $\frac{\pi}{2}$-pulse. A diode was used as detector. Resonance could be detected at around 10 MHz (fig 7.4) and around 5 MHz. Two times around 5 MHz since the splittings in the excited state are 4.59 MHz and 4.84 Mhz (fig 5.2). No resonance around 17 MHz was detected. It is very hard to tell if the 10 MHz resonance comes from exciting atoms to different levels in the excited state or if its resonance between the ground state levels.

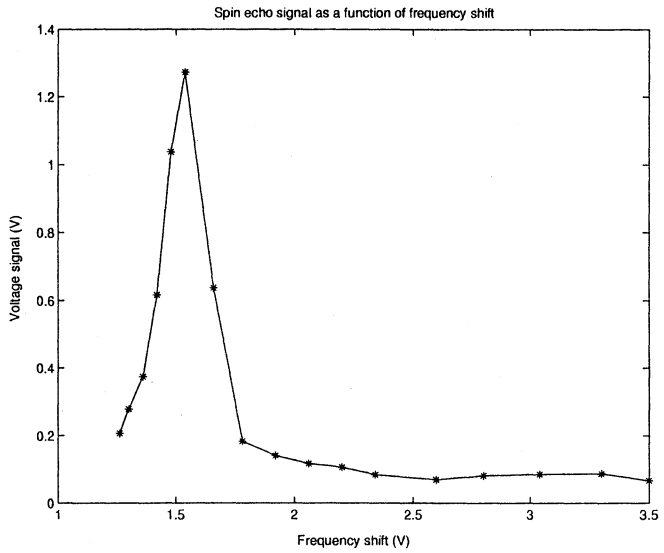

Figure 7.4: The figure shows the three-pulse echo signal as a function of frequency. A peak is clearly visible around 1.6 volt, which with two AOMs correspond to a frequency shift of 10 MHz for the second pulse.

The second part was an attempt to measure the coherence time for the hyperfine levels. The separation of pulse one and two where kept fixed at 4 μs and the delay to pulse three was varied from 20 μs up to 600 μs. Pulse lengths and amplitudes were the same as in the above experiment and the PMT was used as detector.

It is obvious from the data (fig 7.5) that something happens when you shift the second pulse, but the data is not useful at all, especially if you compare with fig 7.6. No conclusions can be drawn. Other then that this experiment did not work.

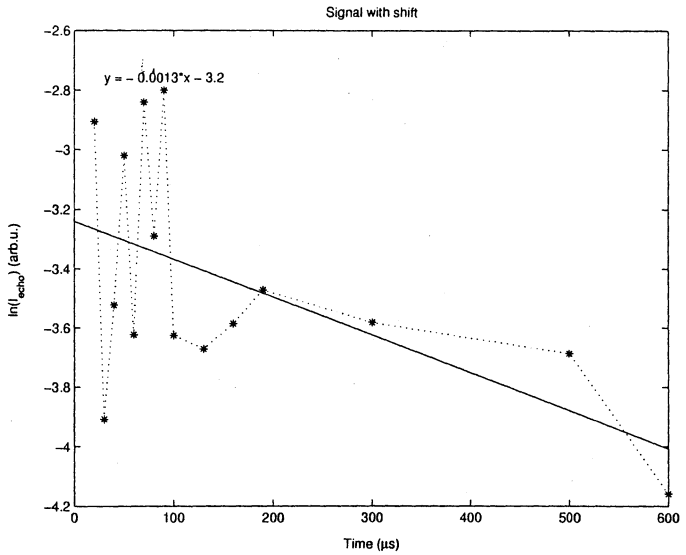

Figure 7.5: The logarithm of the amplitude of the echo plotted against the separation of pulse two and three. The second pulse is shifted 10 MHz. The data possibly suggest a coherence time of about 1 ms.

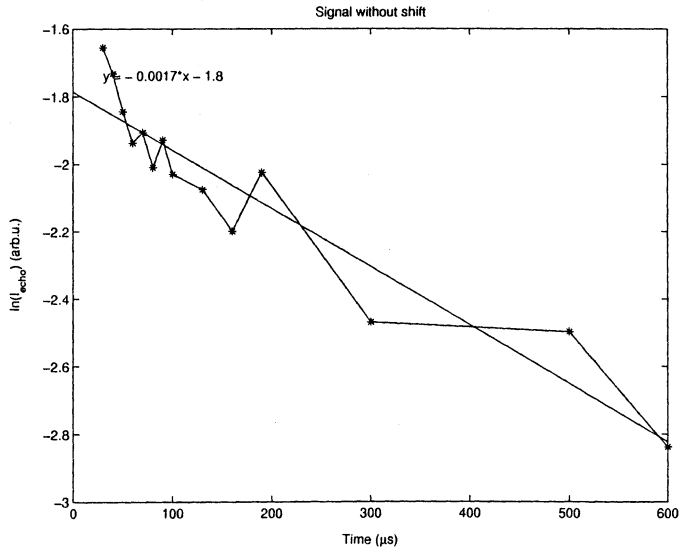

Figure 7.6: The logarithm of the amplitude of the echo plotted against the separation of pulse two and three again. But this time the frequency of the second pulse is the same as the frequency of the first and the third pulse. This data also suggest a coherence time of about 1 ms. Thus no conclusions about the hyperfine coherence time can be drawn from the data in fig 7.5.

7.3 Discussion

A serious drawback with the data displayed in Fig 7.4-7.6 is that it is impossible to determine whether we are looking at the right signal, i.e. the hyperfine level coherence, since we do not know what frequency the echo has. In fact we believe that the detected signal is probably mostly from a gratings with very long lifetime that have been burned into the material in combination with the lifetime of the excited state. This would explain that you get about the same relaxation time even if you do not shift the second pulse. The signal without shifting the second pulse is one magnitude higher though. By applying the shifted second pulse you will destroy the normal three-pulse echo and thus it is expected that you get a stronger signal from the normal three-pulse echo. One other possible explanation could be that the shifted second pulse also excites some ions that are not on resonance. Having a square pulse in the time domain give you a sinc-function (fig 7.7) in the frequency domain that contain frequencies 10 MHz away.

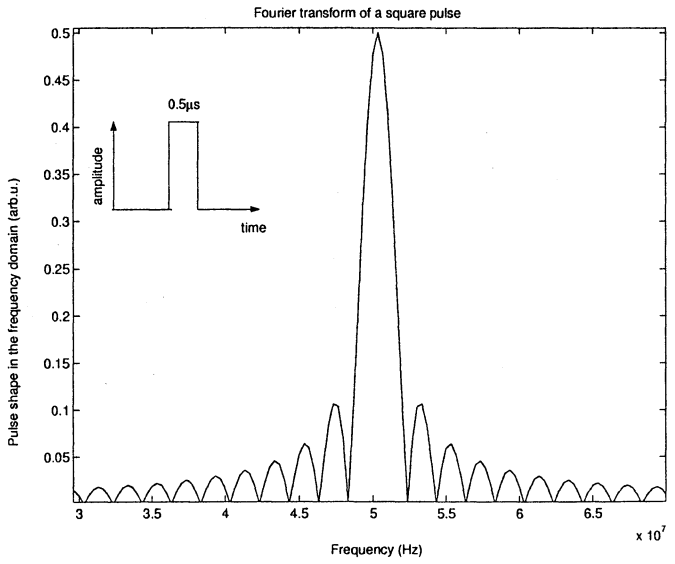

Figure 7.7: The Fourier transform of a square pulse. There might be some contribution from frequencies 10 MHz away in the sidelobes of the sinc-function. This is at most 1% of intensity of the main frequency.

Chapter 8

Spin-coherence heterodyne detection

Heterodyne detection is a sensitive detection where you can both get good signal-to-noise ratio and also determine what optical frequency the signal has. The idea of heterodyne detection is to add a weak laser pulse when the signal is supposed to come. If this weak laser pulse is shifted in frequency compared to the signal you want to measure there will be a beat pattern on the readout pulse. FFT enables you to distinguish the signal, determine the frequency of the beat signal and get really good signal-to-noise ratio.

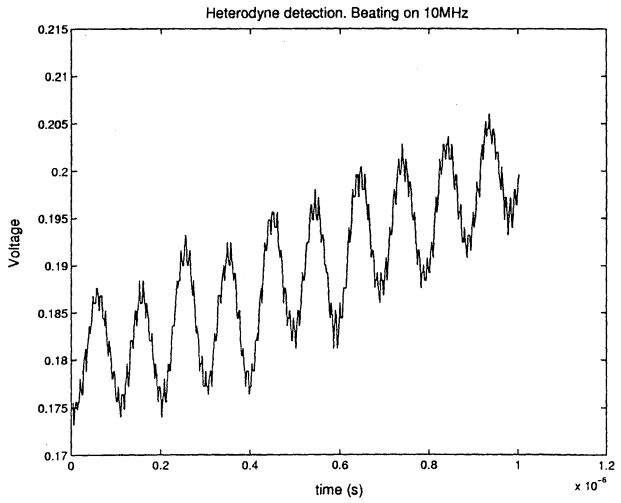

Figure 8.1: The diagram shows a beat between a weak pulse at the $|e> -|1>$ frequency and the echo that has got a different frequency since the second pulse is shifted with 10 MHz. The slope of the curve is due to saturation.

Fig 8.1 is a typical heterodyne signal. Using FFT and looking at the frequency

content of the signal you clearly see the signal (fig 8.2), with almost a noiseless background and you can determine the frequency of the beat.

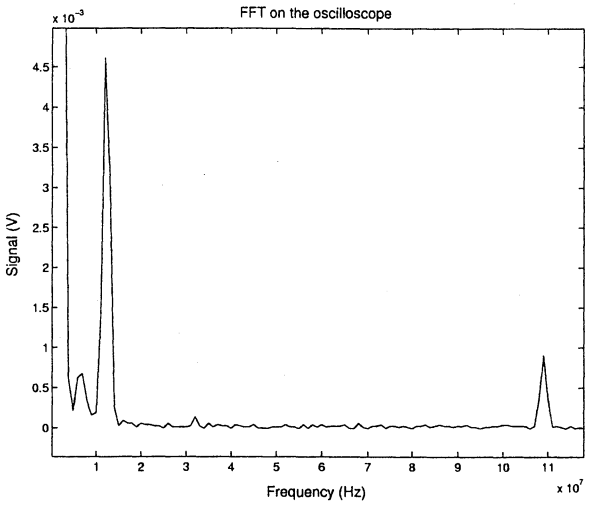

Figure 8.2: Using FFT on the above data you get the echo around 11 MHz with almost no background. Another peak is clearly visible around 107 MHz, which is Radio City 107 MHz that transmits at that frequency.

8.1 Experiment

The experiment is the same as that described in chapter 7 but an additional weak pulse is added when the echo is expected to come. The echo and the weak pulse create a beat pattern that can be detected on the oscilloscope, this is the heterodyne detection. The weak fourth pulse was generated with a SRS DG535 synthesised function generator. The Hamamatsu, $S1223$ photo diode and the PMT were fast enough to detect the beating.

8.2 Results and discussion

Again I did not find any resonance at 17 MHz, but the resonance at 10 MHz and 5 MHz were still there and now I knew for certain that the signal was at the expected frequency and it was therefore most likely the signal I was looking for. Data sequences for the resonance around 10 MHz was taken with both the PMT and the photo diode and they showed similar results. The measured coherence lifetime was discouragingly low. The approximate value was only around 80 μs and the expected value was 500 μs or more. The data gathering could only be done manually at this time and since averaging cannot be performed directly on the oscilloscope when it is operating in FFT mode, each shot had to be saved.

This was a very slow process and drift in the laser frequency or amplitude could become very large over the data collection time. Further measurements therefore had to be automated.

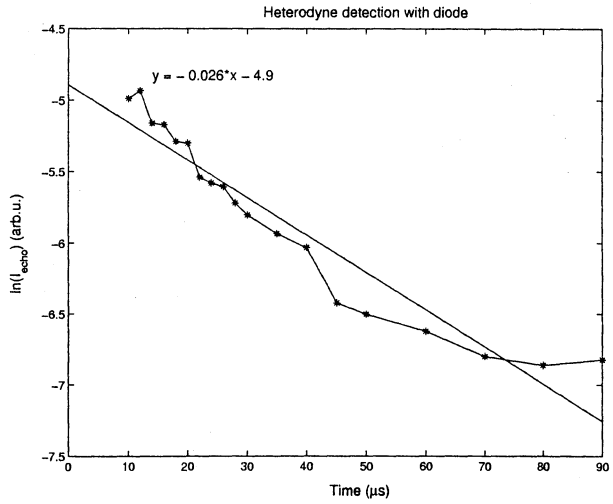

Figure 8.3: The 10 MHz signal plotted in a log diagram against the separation of pulse two and three yielding a relaxation time of about 80 μs. The diode was used as detector.

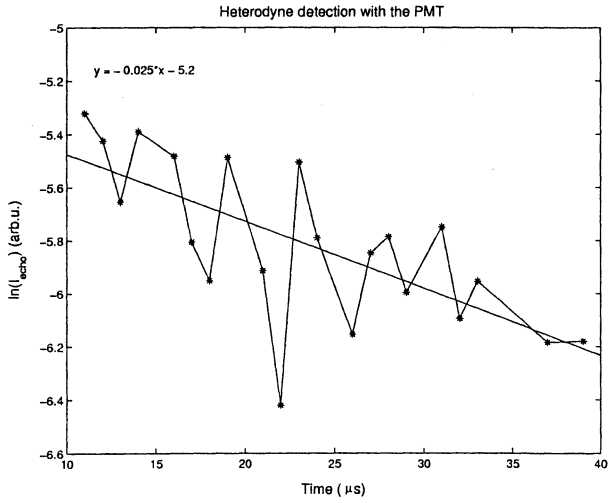

Figure 8.4: The 10 MHz signal plotted in a log diagram against the separation of pulse two and three. The measured value for the relaxation time in this graph was also around 80 μs. The PMT was used as detector. The PMT was much noisier than the diode. The PMT could not be used to its full potential, since I had to add the weak readout pulse during the echo.

Chapter 9

Spin-coherence excitation using temporally overlapping Raman pulses

A new attempt to measure the spin coherence was done using collinear beams. The idea is to apply both frequencies at the same time and in that way create temporally overlapping Raman pulses that excite the coherence. This will eliminate the problem with the inhomogeneous spin broadening that probably was the reason that the first two experiments did not work. It is likely that the inhomogeneous spin broadening caused dephasing if the inhomogeneous line width and the inhomogeneous spin line width were not correlated. The experiment proposed by Babbitt [15] was based on experiments with gases where the inhomogeneous line widths in the excited states and in the ground states are correlated, since they are Doppler broadened. The coherence will be detected with heterodyne detection again, but this time the weak readout pulse will be resonant with some other transition for the ions. From previous experiments it seems obvious that you want to create the coherence between the $\frac{1}{2}$ and the $\frac{3}{2}$ hyperfine levels since it seems like the $\frac{5}{2}$ level does not allow optical transitions to other spin states or at least the transitions are much weaker. This has been indicated throughout my experiments when I have found no signal around 17 MHz. This confirms the results in a recent paper by J.J. Longdell et al. [34] who have also experimentally determined the overlap between the nuclear states, from which you can calculate the oscillator strength between the different hyperfine levels.

The first pulse in the sequence (fig 9.1) is supposed to empty one hyperfine level. If that is not done you will create two coherences between the levels that are out of phase with each other (fig 9.2). Since both processes are possible when you apply a Raman pulse, one that goes from $\frac{1}{2} \rightarrow \frac{3}{2}$ and the other that goes from $\frac{3}{2} \rightarrow \frac{1}{2}$. Then there are two pulse pairs that will work as Raman pulses, shifted 10.19 MHz from each other to be resonant with the hyperfine splitting in the ground state (fig 5.2). The last readout pulse is shifted 5 MHz to be resonant

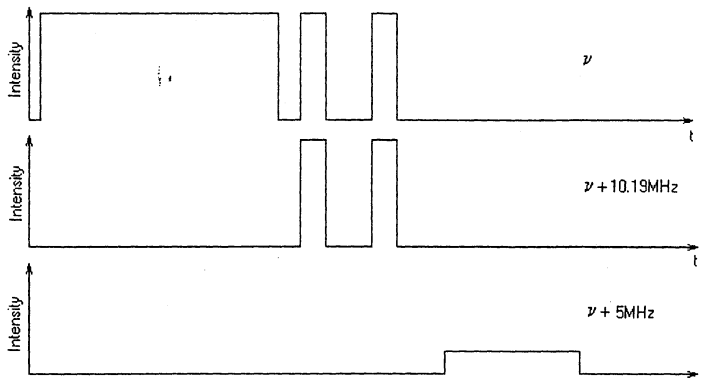

Figure 9.1: Pulse sequence for measuring the coherence time. Two overlapping beams are used in the experiment. One beam path is used to empty one hyperfine level, create two pulses and at last to be used as a readout pulse. The second beam path is used to create two pulses. The first long pulse on ν will empty one of the hyperfine levels that I will use. Then I apply two pulses on both frequencies after each other. The last pulse is the readout pulse that is shifted 5 MHz to be resonant with the spin coherence.

with some other transition for the ions.

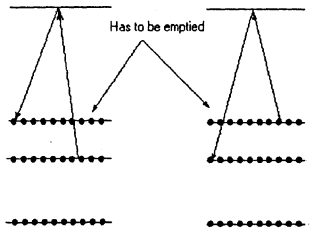

Figure 9.2: You have to empty one of the hyperfine levels to avoid destructive interference.

9.1 Experimental set-up

Two beams are needed in this experiment to create Raman pulses, so the experiment includes two beam splitters and three AOMs to create the necessary pulses. The pulse sequence in fig 8.1 was generated with a TGA1244 arbitrary waveform generator, a DG535 arbitrary waveform generator, a DS345 synthesised function generator, a HP8003A pulse generator and a HP8013B pulse generator. The electronic set-up is explained in more detail in Appendix A. The Hamamatsu, $S1223$ diode was used to detect the signal and a LabView program was written to automate measurements by controlling the DG535.

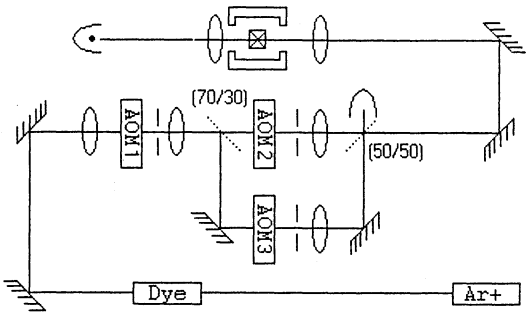

Figure 9.3: Two beam splitters are used to create two beam paths and then overlap them again. The first is 70/30 and the second is 50/50. The choice of a 70/30 beam splitter is motivated by the fact it is harder to make the transition from $\frac{3}{2} \rightarrow \frac{1}{2}$ than $\frac{1}{2} \rightarrow \frac{1}{2}$. Even though it was mostly because I had no other beam splitter, I still think that the asymmetry between the beam strengths was good. Three AOMs are used to create pulses for the two overlapping beam paths. A diode is used for detection.

9.2 Results

9.2.1 Heterodyne detection

Heterodyne detection was used in all four experiments that will be described in this chapter. A typical heterodyne (fig 9.4) signal will be discussed in this section and the Fourier transform (fig 9.5) of the signal will be analysed. The typical shot was taken 10 μs after applying a Raman pulse. The readout pulse was shifted 5 MHz.

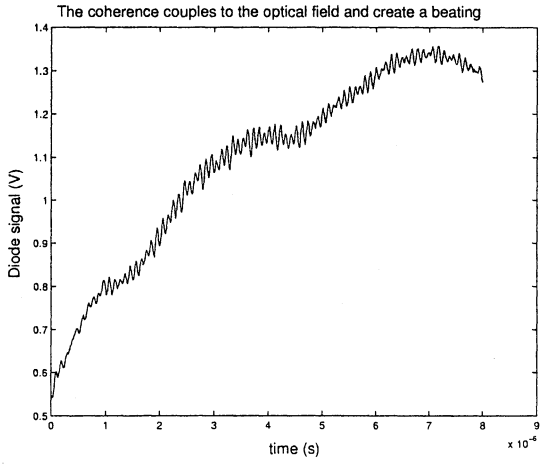

Figure 9.4: The picture is a typical heterodyne detection signal.

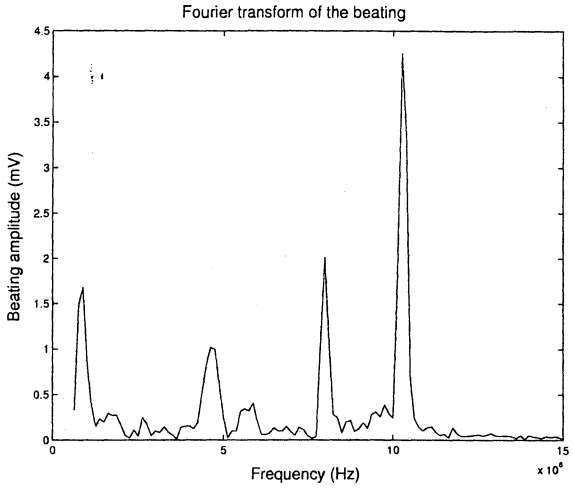

Figure 9.5: The Fourier transform of the heterodyne signal.

The beating is clearly visible in fig 9.4. You can also see that the absorption decreases with time on the readout signal, which indicate that we burn some of the ions away. To get a good signal-to-noise ratio you have to make a trade off between having a long readout pulse and having just one short strong readout pulse. The strength of the beat signal would scale linearly with the intensity of the readout beam, but noise increased as well. Having a longer weaker readout pulse enabled me to make the Fourier transform (fig 9.5) on a larger interval which gave me a better signal-to-noise ratio. I also used a Hanning window to remove the lower frequencies. The peak at 10.19 MHz is well above the noise. There are also peaks at 7.7 MHz, 5.2 MHz and 4.9 MHz (fig 9.5). The peak at 7.7 MHz comes from light leaking through AOM 3 that is turned off (fig 9.6). Peaks at 5.2 MHz and 4.9 MHz are free induction decay from the Raman pulses. The frequency at ν is shifted 5 MHz compared to the frequency of the readout pulse and the frequency at ν+10.19 MHz is shifted 5.2 MHz from the frequency of the readout pulse.

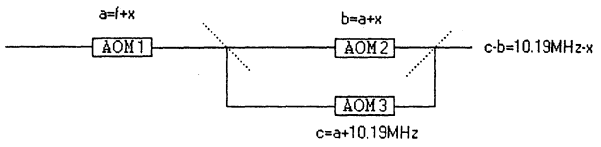

Figure 9.6: AOM 1 and AOM 2 are driven by the same AOM driver and they are both open during the readout pulse. During the readout pulse they get shifted by a voltage so that together they will shift the light with 5 MHz or 2.5 MHz each. AOM 1 also let light through to AOM 3, which is supposed to be turned off. Light that do leak through AOM 3 (shifted 2.5 MHz by AOM 1) is shifted another 10.19 MHz. The frequency difference between the output of AOM 3 and AOM 2 then becomes $10.19 - 2.5 = 7.7$MHz.

9.2.2 Spin coherence coupling to an optical field

A coherent superposition oscillates at a frequency equal to the splitting between the hyperfine levels. Probing the coherence with a weak resonant field will generate a beat signal. The magnitude of this beat signal tells how strong the macroscopic coherence is. The beat frequency will be equal to the energy splitting between the levels. The first step in the experiment was to determine how well the coherence would couple to an optical field. In this experiment there was one burning sequence, one Raman pulse was applied and then the coherence was detected with a readout pulse that was varied in frequency. The delay to the readout pulse was not varied.

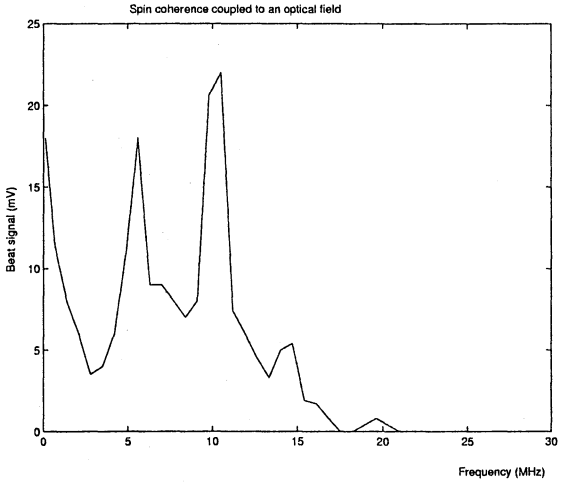

Figure 9.7: The probing field couples much more efficiently to the excited spin coherence if it is resonant with the atoms.

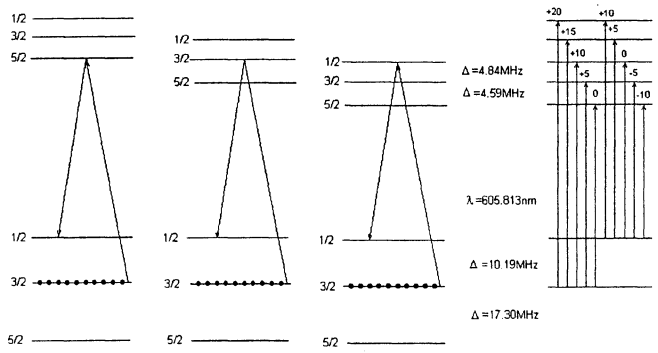

Figure 9.8: Spin coherence coupling to an optical field. It is three possible combinations for coherence excitation as shown in the left figure. Then it is several different resonant cases for the readout beam as shown in the picture to the right.

The field couples strongly when you are on resonance with the atoms. Peaks where found at 0 MHz, 5 MHz, 10 MHz, 15 MHz and 20 MHz (fig 9.7). Which corresponds to five out of seven possible different resonances with three different possible combinations for coherence excitation (fig 9.8). It is just five since I only changed the frequency of the readout beam positively. You can see that the peak at 20 MHz is much lower than the other and it is lower since the $\frac{3}{2} \rightarrow \frac{5}{2}$ and the $\frac{5}{2} \rightarrow \frac{1}{2}$ optical transitions are very weak. I do not want to draw any conclusions of the oscillator strength from this experiment, but this could give ideas for experiments if you want to determine the oscillator strengths. This experiment was not designed for calculating the oscillator strengths for the different optical transitions. The readout beam had to be shifted in frequency since otherwise I get light leaking through the other AOM, controlling the second beam, that is shifted to exactly 10.19 MHz which is the signal I am looking for.

9.2.3 Free induction decay of the spin coherence

With the Raman pulse you create a coherent superposition or a magnetic dipole that oscillates at 10.19 MHz. But all atoms do not oscillate at the same frequency due to the inhomogeneous spin broadening between the hyperfine levels. This will cause the magnetic dipoles to get out of phase with each other just like in a normal photon echo experiment. This gradual dephasing of the signal is called free induction decay. The lifetime of the free induction decay is determined by the width of frequencies you excite. In a normal photon echo experiment you are typically limited by the laser line width or the length of the pulses. The laser line width is 1 MHz and a 500 ns pulse would be roughly 2 MHz wide in frequency, the lifetime of the free induction decay is then about 1 μs. The inhomogeneously spin broadening is expected to be a couple of 10 kHz, so we should be able to detect the free induction decay up to 50 μs or more.

This experiment was done with one long burn pulse, only one Raman pulse and a weak probe pulse. The burning sequence was 360 μs long with a 700 μs delay until the Raman pulse, to make the diode recover. The laser was swept 0.2 GHz/s during the experiment and the output was 19.2 mW and 37.2 mW (shifted 10.19 MHz) for the two overlapping beams. A 10 cm lens focused the beam onto the crystal. The readout pulse was as weak as possible to avoid burning any atoms away, but still strong enough to give a reasonable signal to work with. The data was collected by a repeated measurement controlled by a computer. Each data point then corresponds to an average of 40 measurements (fig 9.10). With the results from this experiment it was possible to determine with a simulation that the inhomogeneous line width was 16 kHz (fig 9.11) if you assumed a Gaussian profile. This is quite surprising since *Holliday et al*[23] have reported 30 kHz. *Ham et al*[30][29][27] on the other hand have reported a line width that spans from 15 kHz to 40 kHz.

The spin broadening might be sensitive to the magnetic environment for the crystal. It appears that the only magnetic field that interact with the crystal should be earths magnetic field in this case. It might then be some difference when doing experiments at MIT (Ham's group), Switzerland (Holliday's group) and here in Lund. Other possible perturbations could be magnetic dipole-dipole

interaction, electric dipole-dipole interaction and electric dipole-quadrupole interaction with the surrounding lattice. You would then have different energies depending on the nuclear states of the ions neighbours. These are rather dynamic processes then static processes and would hence be reasons for decoherence, but it might as well be a coin with two sides and explain both the decoherence and the inhomogeneous line width.

When the Pr^{3+} ion change its spin state it is quite likely that the surrounding Y^{3+} will flip also. There are a lot of superhyperfine levels for the Pr^{3+} that depend on the neighbouring nuclear states of Y^{3+}-ions. If you apply a magnetic field the energy to make a spin transition for Y^{3+}-ions increases and when this energy is larger then the Pr-Y interaction you will no longer flip any Y^{3+}-ions when you flip the spin for the Pr^{3+}-ions[36]. The inhomogeneous line width might then decrease if you apply a magnetic field. Using this model it can be very hard to distinguish the inhomogeneous spin line width from the homogeneous spin width since they are of the same order and the effects that cause the inhomogeneous and homogeneous broadening are similiar. There will still be static effects in the lattice, that will cause an inhomogeneous broadening, like imperfections and impurities. A Pr^{3+}-ion that is located close to, e.g., an iron ion will feel a different magnetic environment then a Pr^{3+}-ion that is just surrounded with Y^{3+}-ions.

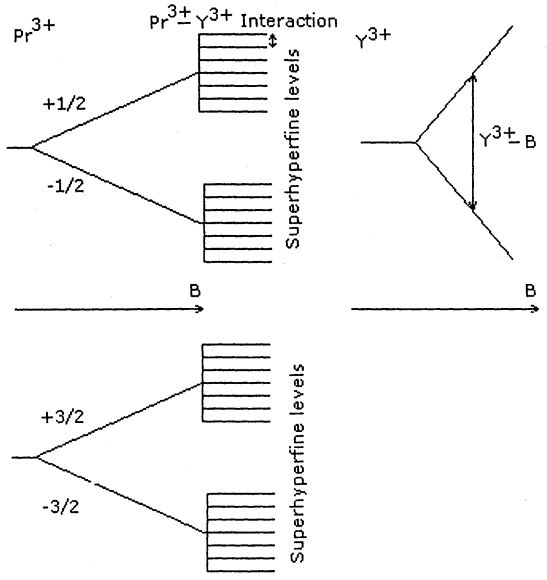

Figure 9.9: The picture shows the energy diagram for two levels in the ground state for Pr^{3+}. The nuclear states get split in a magnetic field because of the Zeeman effect. These individual lines then splits into superhyperfine levels because of the Pr-Y interaction. The nuclear states of Y^{3+}-ions also splits in a magnetic field. The Pr^{+3}-ions will not be able to flip any Y^{3+}-ions when the interaction between the magnetic field and Y^{3+}-ions is larger than the Pr-Y interaction.

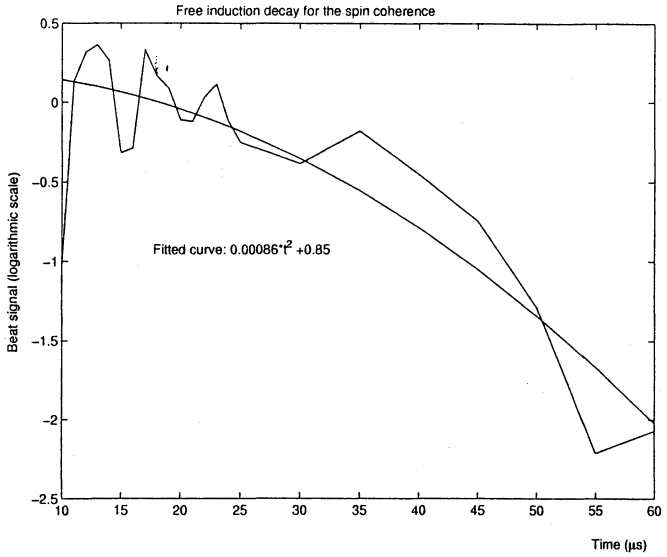

Figure 9.10: The measured free induction decay. The fitted quadratic function suggest that there is a Gaussian inhomogeneously spin line width. By simulating how light is transmitted from ions that are distributed in a Gaussian profile it was possible to recreate the fitted quadratic decay in the diagram. Which give the Gaussian profile of the inhomogeneous line width.

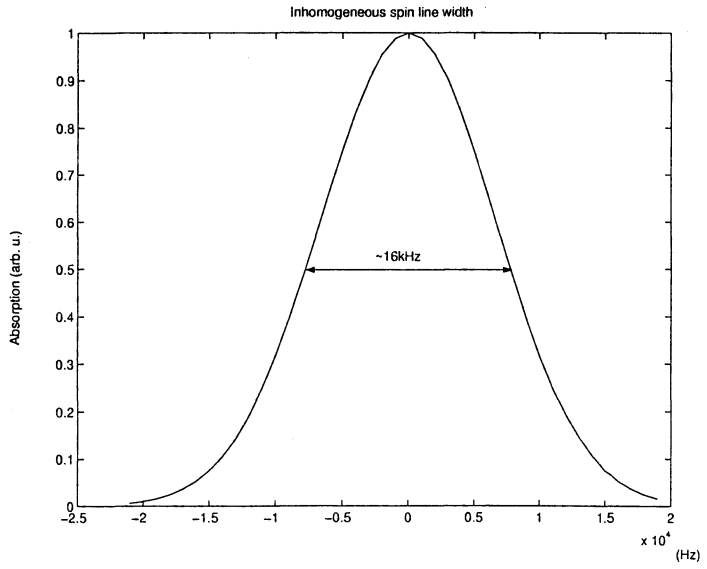

Figure 9.11: The simulated Gaussian profile.

9.2.4 Coherence time measurement

In the next experiment I use the same parameters as above but adding a second Raman pulse. This pulse is applied to make the atoms rephase again and give a spin echo. The time between the Raman pulses and the time to the readout pulse were varied and a plot of the spin echo signal versus time will give you the loss of coherence or the coherence time. The readout pulse was shifted 4.7 MHz to be on a resonance with the coherence. The pulse-lengths[1] where 1200 μs and 1400 μs. The data was again collected using a repeated measurement controlled by a computer. Each data point now correspond to an average of 50 measurements.

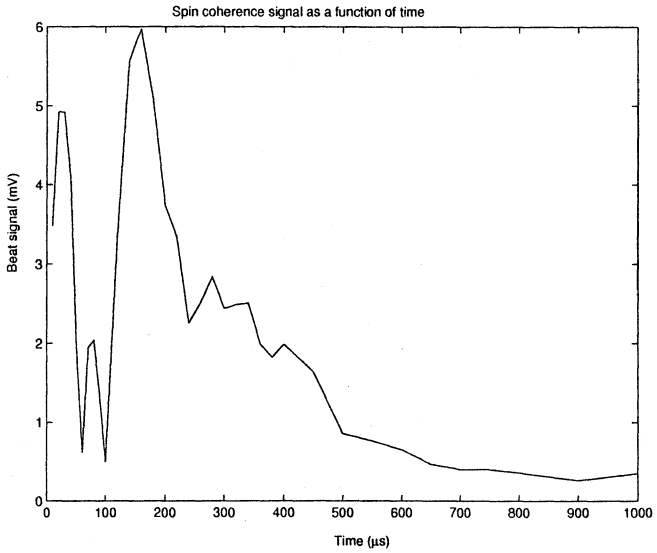

Figure 9.12: The picture shows the detected spin coherence signal. The first 100 μs cannot be used. There are several other effects you have to consider that takes place in that regime as discussed in the text.

The first 100 μs cannot be used (fig 9.12). There are other effects you have to consider that takes place in that regime. First of all the second Raman pulse excites another coherence that is out of phase with the original spin coherence that you intend to rephase. The first Raman pulse makes the transition from $\frac{3}{2} \rightarrow \frac{1}{2}$ and when you rephase those with the second Raman pulse you want to make the transition $\frac{1}{2} \rightarrow \frac{3}{2}$. But you will also again make the transition $\frac{3}{2} \rightarrow \frac{1}{2}$ for some ions. Those spin coherences will be out of phase with each other. You also get two normal two-pulse echoes that create a 10.19 MHz beat frequency with each other. That signal should decay quadratically with the optical coherence that is 111 μs [22]. A normal two-pulse echo will decay as:

$$I = I_0 e^{-\frac{4t}{T_2}} \tag{9.1}$$

[1]The experiment seemed to be very sensitive to the pulse area of the excitation pulses. Thus it seemed to be really important that you had π- and $\frac{\pi}{2}$-pulses.

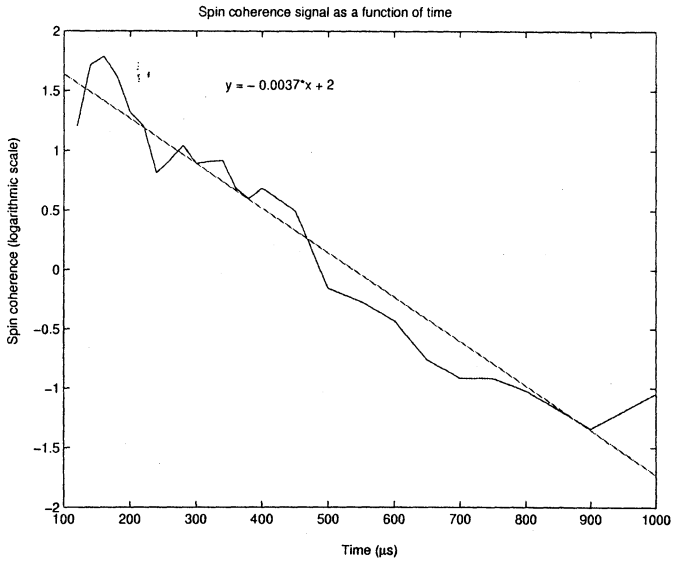

Figure 9.13: The diagram shows a logaritmic plot of the signal versus time for the signal beyond 100 μs. From the diagram you can read out that the coherence time would be 540 μs.

If you have two two-pulse echoes that create a beat against it will decay as

$$I = (I_0 e^{-\frac{4t}{T_2}})^2 \tag{9.2}$$

The lifetime of the excited state is 164 μs[22] so you might have some effect due to that as well. Those are effects that I can come up with that could in some way contribute to the minimum around 100 μs. Figure 9.13 shows a logarithmic plot of the signal versus time for the signal beyond 100 μs. The measured coherence time was 540 μs. The spin coherence is assumed to decay as:

$$E = E_0 e^{-\frac{2t}{T_2}} \tag{9.3}$$

In this case we do not measure the intensity of a spin echo and the measured spin coherence become proportional to the measured beat signal. Looking at the equation $\frac{2}{T_2}$ is then equal to 0.0037, which give the coherence time. The measured value 540 μs is fairly long for a solid state material, but coherence times of up to 3 ms have been reported in $Eu : Y_2SiO_5$ [17].

9.2.5 The Spin echo width

In this experiment the time between the two Raman pulses were kept fixed but the time to the readout pulse was varied. The readout pulse will work like a sliding window that moves over the echo and you will be able to see the atoms first rephase into an echo and then start to dephase again after the peak of the echo signal.

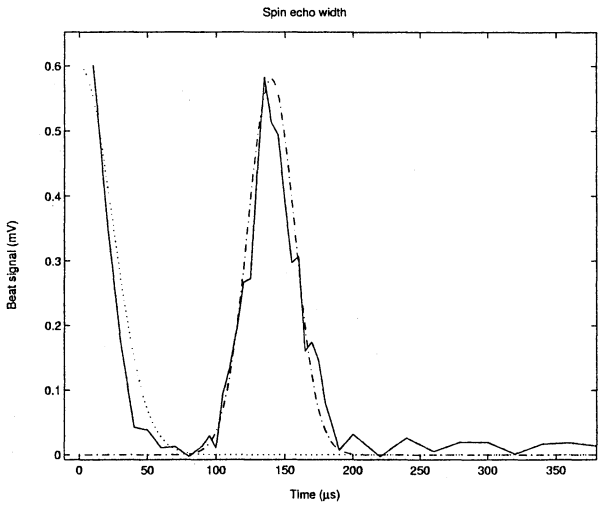

Figure 9.14: The diagram shows the result. The separation between the Raman pulses is 140 μs. The free induction decay in the beginning is due to another coherence that is created by the second Raman pulse. The second pulse also rephase the original coherence and they form an echo after 140 μs. Using the results from the spin free induction decay section I was able to simulate the free induction and the spin echo. Those are the dotted curves in the diagram and they seem to agree quite well with experimental data.

The reason for the free induction decay is that the ions get out of phase with each other since they are distributed with a Gaussian frequency profile. Doing a simulation of oscillating dipoles within that Gaussian profile that send out light you are able to see them dephase and the signal decreases. The free induction decay in the beginning of the diagram is simulated with that kind of process, with variables taken from section 9.3.3. When the ions start to rephase you have the opposite effect until the echo where they are all supposed to be in phase with each other. After the peak of the echo you will get free induction decay again. The echo is created with the same processes that give the free induction decay. It is then a simple simulation once you have the numbers.

$E_{FID} = E_0 e^{-at^2}$
$E_{ECHO} = E_1 e^{-a(t-140)^2}$

Where a is the number taken from fig 9.10, $a = 0.00086$ and 140 is in μs. E_0 and E_1 were normalised to be the peak value of the free induction decay and the echo respectively. The width of the echo is then approximately 50 μs.

9.3 Conclusions and reflections

The last experiment left no doubt though, it had to be the coherence I measured. There was no way to get the signal if I did not use the right pulse sequence and frequency splitting. The measured inhomogeneous spin broadening also explained why the experiment in chapter 8 did not work. Looking back at the data and trying to fit a quadratic function to the decay of what I thought was the coherence, it give approximately the same decay function as the one for the spin free induction decay.

The measured values are also consistent with values that Ham et al. [30] has reported. The set-up for their experiment was quite different though. And in my opinion it is a much more complicated experiment. Their experiment is explained briefly below.

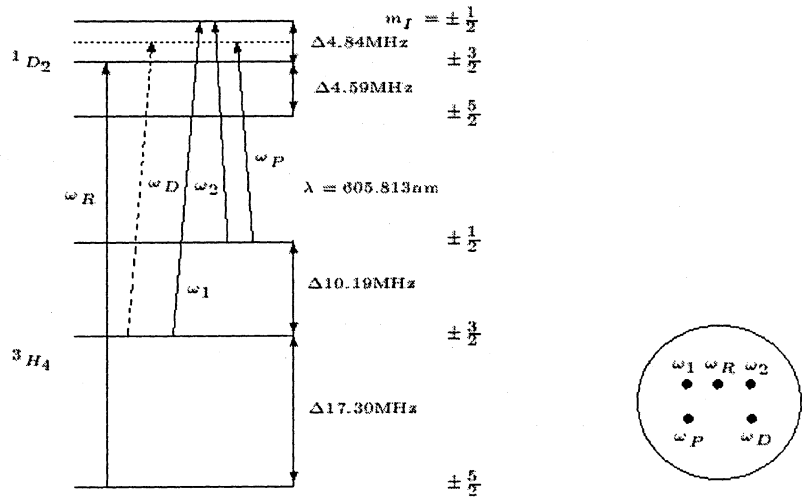

Figure 9.15: The left picture is the energy level diagram of $Pr^{3+} : Y_2SiO_5$ with the transitions that Ham et al used in their experiment. The right picture shows the schematic geometric picture of their laser beam arrangement.

The *Raman* resonant laser fields are ω_1 and ω_2. The field at ω_R is used to repump atoms that would otherwise accumulate in the $\frac{5}{2}$ state. A probe ω_P is used for detection of the ground state spin coherence. This probe is detuned 1MHz from ω_2 and is Bragg matched to diffract light from the ground state coherence grating created by the noncollinear beams ω_1 and ω_2. The diffracted light ω_D from ω_P is then used to probe the ground state coherence because of enhanced nondegenerate four-wave mixing [30][27]. To put it in more simple words, they detect the coherence in a direction different from that of the Raman pulses. The probe beam only gets diffracted if there is a grating in the groundstate that is due to spin coherence.

Doing my experiment again would be quite straightforward, but there are two

improvements that I would like to suggest. The first *Raman* pulse was suppose to work like a $\frac{\pi}{2}$-pulse between the hyperfine levels and the second should have been a π-pulse. When I did run the experiments both pulses where equal in length, so I would expect an increased signal if you make the second *Raman* pulse longer than the first. The other improvement would be to shift the frequency negatively for the readout pulse. In fact I belive that you would have got the strongest signal if you had shifted it to -5 MHz (fig 9.8).

I would also like to propose some future experiments that would use this technique to detect the coherence. The first step would be to apply a magnetic field. The nuclear spin levels do not interact much with the surrounding environment hence the long coherence time. The main reason of decoherence are changing magnetic fields due to nuclear and electronic spins. The spin levels can then mainly be affected by three interactions: magnetic dipole-dipole, electric dipole-dipole and electric dipole-quadrupole interaction. The Pr-Pr and Pr-Y (to some extent also Pr-^{29}Si) interactions are both magnetic dipole-dipole interactions since the spin states have a magnetic dipole moment. On average the Pr-Y ions are situated much closer in lattice and this will be the main perturbation. By applying a magnetic field you should be able to slow down the mutual spin flips between Y^{3+}-ions. This have been done in a recent experiment in Canberra by Annabel Alexander [36] and she has found the coherence time to increase radically if you apply a magnetic field and reported coherence times up to 7 ms. She also mentions that her group has reported up to 82 ms coherence time if you apply the right magnetic field, without discussing what they mean with the right magnetic field. The electric dipole-dipole and electric dipole-quadrupole interactions would only take place if you excite nearby Pr^{3+} ions. But those effects have to be considered later on in the ESQUIRE project. Since doing operations, that includes optical transitions, on two qubits might affect a third qubit.

You could also use rf-coils to create the coherence between the hyperfine levels and in that way create much stronger coherence that would be easier to detect. Having a stronger signal means that you would be able to do very sensitive measurements and find out what causes decoherence in the crystal. On the other hand it is impossible to choose just one channel within the inhomogeneous line, as with the technique developed here.

It should also be possible to make a frequency sweep during the Raman pulses which then should be longer than those that I used. By doing that you will talk to more ions and thus get a stronger signal. The same frequency sweep should also be added to the burning sequence. The frequency interval could be around 7 MHz. You cannot add a frequency sweep during the readout pulse, since that would create a lot of extra frequency beats. As can be seen in fig 9.7 you still get a signal when you are not on resonance and those together with the resonant ions should give a stronger signal. I tried this experiment, but I could not see any improvement. On the other hand I attempted to do this when I did not know how to get a strong signal and by adding the frequency sweep it just felt like one parameter to much and way too much electronics.

Chapter 10

Conclusions and outlook

The experiments in chapter 9 worked out surprisingly well, especially after having to face the disappointments while doing the preceeding experiments. The measured values are consistent with two other experiments[36][30] that have been done differently. The Pr^{3+}:Y_2SiO_5 crystal has a large oscillator strength and not too large hyperfine-splittings. This made the crystal easy to work with, but the method to measure the coherence time should be easy to adapt to other RE-crystals as well. The hyperfine levels coherence time in Pr^{3+}:Y_2SiO_5 is also sufficiently long if you consider the quantum computer scheme. The problem is the ion-ion interaction in the crystal, which is probably not large enough if you want to do scale the system to several qubits. It might be possible to create two or three interacting qubits using this crystal though if you have a good enough laser. This master's thesis also fulfill the requirements for one of the deliverables in the ESQUIRE project. A deliverable for demonstrating a technique for measuring hyperfine coherence times, this deliverable was due 2005. It is also possible that this method could be used to improve data storage in RE-crystals[30]. Since the coherence time between the hyperfine levels are much longer then the coherence time for the optical transitions. Further excitation induced frequency shifts would not affect the spin coherence in the same way as for normal photon echoes, since that is caused by an electric dipole-dipole interaction. The electric dipole-dipole moment induced by other excited Pr^{3+}-ions would then just shift both ground state hyperfine levels the same amount and the nuclues would not care. The spin coherence excitation should then be more efficient then normal photon echoes. On the other hand you are still limited by the weak optical transition between different nuclear states, so the signal you would work with is quite small. The coherence time for the hyperfine levels does not decrease as fast as the coherence time for the optical transition when you raise the temperature and it might be possible to do data storage at much higher temperatures[30].

The first steps towards the realisation of the quantum computer scheme has already been successfully demonstrated [33]. But there are still several unresolved questions and experimental techniques to develop. Further research within this field will be carried out in the ESQUIRE project that will last for the next

three years. A first step in the project will be the new laser system that is being developed by Lars Rippe at the division. This system is supposed to be stabilized down to less then 100 kHz. Other possible improvements of the quantum computer scheme would be a new crystal. Crystals with multiple dopants are considered, where one element can be used as qubits and the other as qubit buses[37]. Better understanding on what causes decoherence in a crystal is also needed. I think that if you understand the process that give decoherence then you are also able to limit them.

The quantum information society is expanding each day and new experimental and theoretical results in the field are presented almost every week. It is hard to predict which road to take but I think this quantum computer scheme is highly competitive with other schemes. The current roadmap for quantum computers expect someone to be able to create 50 interacting qubits within 10 years. The ESQUIRE goal is to manage to create more than two within those 3 years the project spans. If that goal is achieved then I do not think it should be to far off to be able to create 50 qubits within 10 years. Even if that is a question of how good scalability this system would have.

Chapter 11

Acknowledgements

I would like to thank my supervisor Stefan Kröll for introducing me to and giving me the opportunity to work in such fascinating area as this. I would further like to thank the rest of the photon echo group, Mattias Nilsson, Lars Rippe and Nicklas Ohlsson, for all their help, support and interesting ideas. I am most grateful for always taking time to and try to answer my questions, and there have been plenty of questions. I would also like to thank Mattias further since you had to help me so much in the laboratory.

I do not want to thank the dye laser that seems to live its own life. The cryostat that we worked on for at least two months without getting it to work. Electronic equipment that did not work, coaxial cables that were broken and everything that makes the life of an experimentalist hard. To whatever ghost that sneaks around during the night changing the dye laser, just stop haunting us!

It is been a lot of late nights, early mornings, working weekends and dissappointments. But I do not regret it at all! I've gained a lot of experience while working with the equipment and I've learned some theory as well. In the end I am quite proud of what I've managed to do in just six months.

Finally I would like to thank everyone not mentioned above but that have helped me during this project.

Bibliography

[1] Robert W. Boyd. *Nonlinear Optics.* Academic Press (1992).

[2] Dirk Bouwmeester, Artur Ekert and Anton Zeilinger. *The Physics of Quantum Information.* Springer-Verlag (2000).

[3] Andrew Steane. *Quantum Computing.* Rep. Prog. Phvs. **61** 117-173 (1998)

[4] P.W. Shor. *Polynomial-Time Algorithms for Prime Factorization and Discrete Logarithms on a Quantum Computer.* quant-ph/**9508027** (1996).

[5] L.K. Grover. *A fast quantum mechanical algorithm for database search.* quant-ph/**9605043** (1996).

[6] A. Barenco, D. Deutsch and A. Ekert. *Conditional Quantum Dynamics and Logic Gates.* Physical Review Letters **74**, 4083 (1995).

[7] Andrew Steane. *Error correcting codes in quantum theory.* Physical Review Letters, **77**, 793 (1995).

[8] V. Giovannetti, D. Vitali, P Tombesi and A. Ekert. *Scalable quantum computation with cavity QED systems.* Physical Review A **62**, 032306 (2000)

[9] S. Svanberg, *Atomic and Molecular Spectroscopy,* 3^{rd} *ed.* Springer-Verlag, (2001).

[10] T.D. Ladd, J.R. Goldman, F. Yamaguchi, Y. Yamamoto, E. Abe and K.M. Itoh. *All-Silicon Quantum Computer.* Physical Review Letters **89** 017901 (2002).

[11] N. Ohlsson, R.K. Mohan and S. Kröll, *Quantum Computer Hardware based on Rare-earth-ion doped Inorganic Crystals.* Optics Communication **201**, 71 (2001).

[12] R.M. Macfarlane, R.M. Shelby. *Coherent Transient and Holeburning Spectroscopy of Rare Earth Ions in Solids.* Spectroscopy of Solids, (1987).

[13] E.L. Hahn. *Spin Echoes.* Physical Review, **80** 580 (1950)

[14] N.A. Kurnit, I.D. Abella and S.R. Hartmann. *Radiation locked photon echoes and optical free-induction in ruby.* Physical Review Letters, **13**, 567 (1964)

[15] W.R. Babbit. *The Response of inhomogeneously broadened optical absorbers to temporally complex light pulses.* PhD thesis, Harvard (1987)

[16] Felix R. Graf, Alois Renn, Gert Zumofen and Urs P. Wild. *Photon-echo attenuation by dynamical processes in rare-earth-ion-doped crystals.* Physical Review B **58**, 5462 (1998)

[17] R.W. Equall, Y. Sun, R.L. Cone and R.M. Macfarlane. *Ultraslow Optical Dephasing in* $Eu^{3+} : Y_2SiO_5$. Physical Review Letters **72**, 2179 (1994)

[18] G.P. Flinn, K.W. Jang, M.L. Jones, R.S. Meltzer and R.M. Macfarlane. *Sample-dependent optical dephasing in bulk crystalline samples of* $Y_2O_3 : Eu^{3+}$. Physical Review B **49**, 5821 (1994)

[19] Ryuzi Yano, Masaharu Mitsunaga, and Naoshi Uesugi. *Stimulated-photon-echo spectroscopy. I. Spectral diffusion in* $Eu^{3+} : YAlO_3$. Physical Review B **45**, 12752 (1992)

[20] Felix R. Graf, Alois Renn, and Urs P. Wild. *Site interference in Stark-modulated photon echoes.* Physical Review B **55**, 11225 (1997)

[21] T. Christiansson. *A first step towards Quantum Computing in Rare-earth-ion-doped crystals.* Lund Reports on Atomic Physics **LRAP-266**, (2001).

[22] R.W. Equall, R.L. Cone and R.M. Macfarlane. *Homogeneous broadening and hyperfine structure of optical transitions in* $Pr^{3+} : Y_2SiO_5$. Physical Review B, **52** 3963 (1995)

[23] Keith Holliday, Mauro Croci, Eric Vauthey and Urs P. Wild. *Spectral hole burning and holography in an* $Y_2SiO_5 : Pr^{3+}$ *crystal.* Physical Review B **47**, 14741 (1993)

[24] G. J. Pryde, M. J. Sellars, and N. B. Manson. *Solid State Coherent Transient Measurements Using Hard Optical Pulses.* Physical Review Letters **84**, 1152 (2000)

[25] Coherent, *Coherent 699-21 ring dye laser manual.*

[26] Frank L. Pedrotti and Leno S. Pedrotti. *Introduction to optics.* Prentice-Hall International Inc. (1996)

[27] B.S. Ham, M.S. Shahriar and P.R. Hemmer. *Enhancement of four-wave mixing and line narrowing by use of quantum coherence in an optically dense double-*Λ *solid.* Optics letters **24**, 86 (1999)

[28] B.S. Ham, M.S. Shahriar, M.K. Kim and P.R. Hemmer. *Frequency-selective time-domain optical data storage by electromagnetically induced transparency in a rare-earth-doped solid* Optics Letters **22**, 1849 (1997)

[29] B.S. Ham, M.S. Shahriar and P.R. Hemmer. *Enhanced nondegenerate four-wave mixing owing to electromagnetically induced transparency in a spectral hole-burning crystal.* Optics Letters **22**, 1138 (1997)

[30] B.S. Ham, M.S. Shahriar, M.K. Kim and P.R. Hemmer. *Spin coherence excitation and rephasing with optically shelved atoms.* Physical Review B **58**, 11825 (1998)

[31] M. Yamaguchi, K. Koyama, T. Suemoto and M.Mitsunaga. *Perturbed ion sites in $Eu^{3+} : YAlO_3$ studied by optical-rf double-resonance spectroscopy.* Physical Review B **59**, 9126 (1999)

[32] H.Hertz and L-Å Nilsson. *Construction and testing of a digital wavelength meter.* Lund Reports on Atomic Physics, **LRAP-2**. (1981).

[33] M.Nilsson, L. Levin, N.Ohlsson, T.Cristiansson and S.Kröll, *Initial experiments concerning quantum information processing in rare-earth-ion doped crystals.* Physical Scripta **T102**, 178-185 (2002)

[34] J.J. Longdell, M.J. Sellars and N.B. Manson. *Hyperfine interaction in gound and excited states of praseodymium-doped yttrium orthosilicate.* Physical Review B **66**, 035101 (2002)

[35] WebElementsTM Periodic table, http://www.webelements.com/

[36] Alexander, Annabel. Investigation of qubit isolation in a rare-earth quantum computer. Honours thesis, Department of Physics, RSPSE, ANU (2002)

[37] Janus Wesenberg, Klaus Moelmer. *Robust quantum gates and a bus architecture for quantum computing with rare-earth-ion doped crystals.* Quant-ph/**0301036**. (2003)

Appendix A

Configuration of Electronics

Several pulse-generators where used to create the optical pulse-sequence (fig 9.1). For each AOM-driver there are two controlling voltages you can alter, V_T and V_{MOD}. V_T is used to change the RF-frequency and by applying a voltage over V_{MOD} you turn the AOM on. In this set-up three different AOMs are used as can be seen in (fig 9.3). AOM 1 and AOM 2 are driven by the same AOM-driver and AOM 3 has its own driver. In this experiment V_{MOD} is controlled for both AOM drivers and V_T is controlled externally only for the AOM driver controlling AOM 1 and AOM 2. V_T is set for both drivers to give a frequency shift between the two beams of 10.19 MHz (fig 9.3). The $DG535$ digital pulse generator was controlled by a computer. A LabView program was written, or rather rewritten, to control the time sequence of the pulses and acquire the data after each shot. The time between the Raman pulses (B and C) and the delay before the readout pulse was changed (C and D) (fig A.1). The LabView program then cycled through a time sequence and made the data acquisition.

The timing of the pulses are given in Table A.1 and the electronic pulses needed for the experiment shown in Fig A.1. At T_0 the pulse sequence start by letting the $DG535$ trigger $HP8003A$ that give an electronic pulse. This pulse is then connected to the *Sum* channel input on the $TGA1244$. The $TGA1244$ then adds this input to $Ch1$ that controlls V_{MOD} for AOM 1 and AOM 2. At time A a pulse from the $DG535$ trigger the $TGA1244$ that generates pulses on $Ch1$ and $Ch2$, which give the *Raman* optical pulse. At time C the $DG535$ again triggers the $TGA1244$ to generate the second *Raman* pulse. The $DG535$ then triggers $DS345$ and $HP8013B$ at time D. The $DS345$ generates the frequency shift for the readout pulse by adding a voltage on V_T for the AOM driver controlling AOM 1 and AOM 2. After a small delay $HP8013B$ generates the electronic readout pulse that is directed to $Ch1$ in the same way as for the burning pulse.

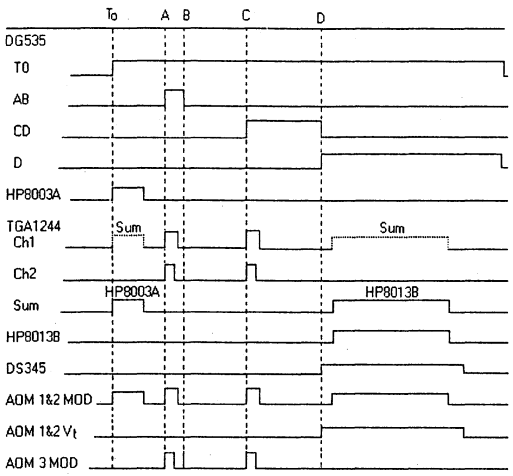

Figure A.1: Pulse sequence for electronics. T_0, A, B, C and D are time parameters that is defined by $DG535$. The equivivalent light pulses are those that are set by AOM 1&2 MOD, AOM 3 MOD and AOM 1&2 V_T, within the limit on how fast the AOMs respond to electric pulses.

Using this set-up you get a electronic pulse sequence that look like this:

Pulse	Time	Duration
T_0	0	
Burn Pulse	0	400 μs
A - T_0	1000 μs	
Ch1	A	1400 ns
Ch2	A	1200 ns
C - A	10 μs – 1 ms	
Ch1	C	1400 ns
Ch2	C	1200 ns
D - C	10 μs – 1 ms	
Readout pulse	D	10 μs

Table A.1: Time sequence for optical pulsses.

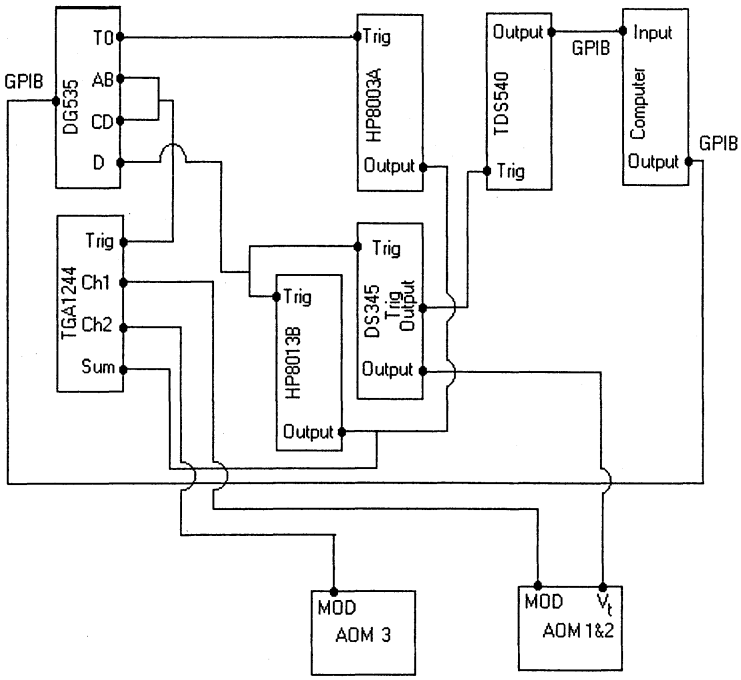

Figure A.2: Set-up for electronics. The oscilloscope and the *DG*535 are connected to the computer via GPIB.